2

phy. The structural features that are required for the inverse agonist properties of some ARBs have been studied in constitutively active AT$_1$ receptors that have an Asn[111] mutation. For example, the ternary interactions between the hydroxyl group of the imidazole ring and Tyr[113] of the AT$_1$ receptor and between the carboxyl group and Lys[199]

and His[256] of the AT$_1$ receptor were required for the inverse agonist activity that olmesartan exerts on GTPase-stimulating activity in a constitutively active AT$_1$-N111G mutant containing an Asn[111] to Gly mutation.[9] However, studies using substituted cysteine accessibility mapping (SCAM) showed that conformation of the AT$_1$ receptor
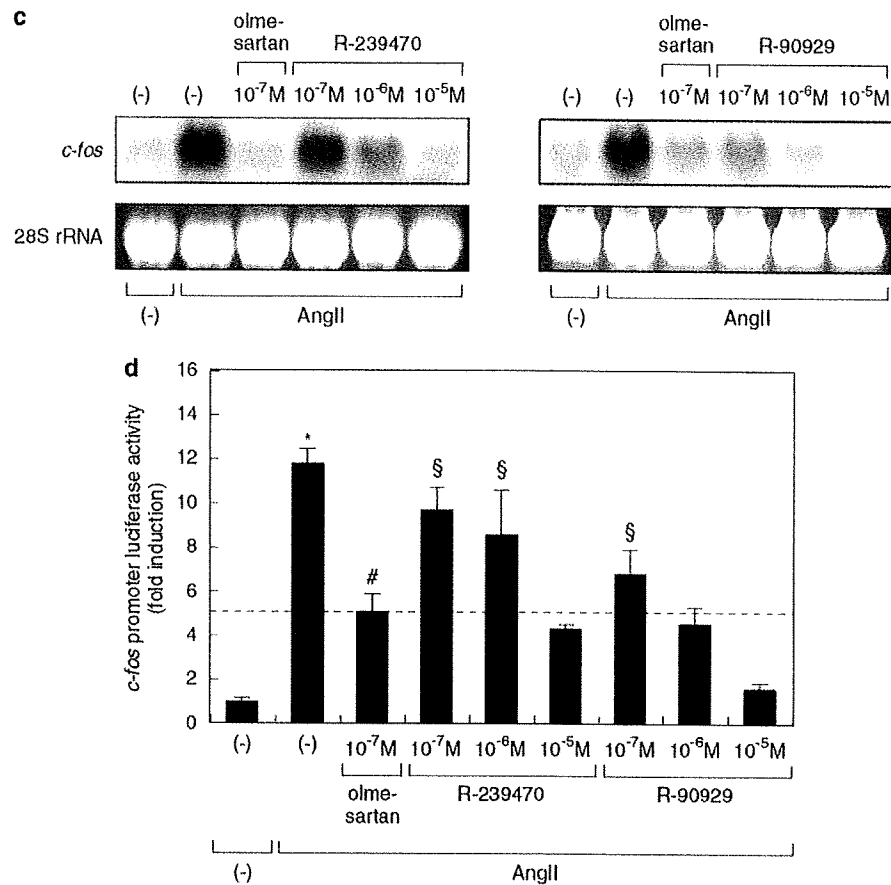
39
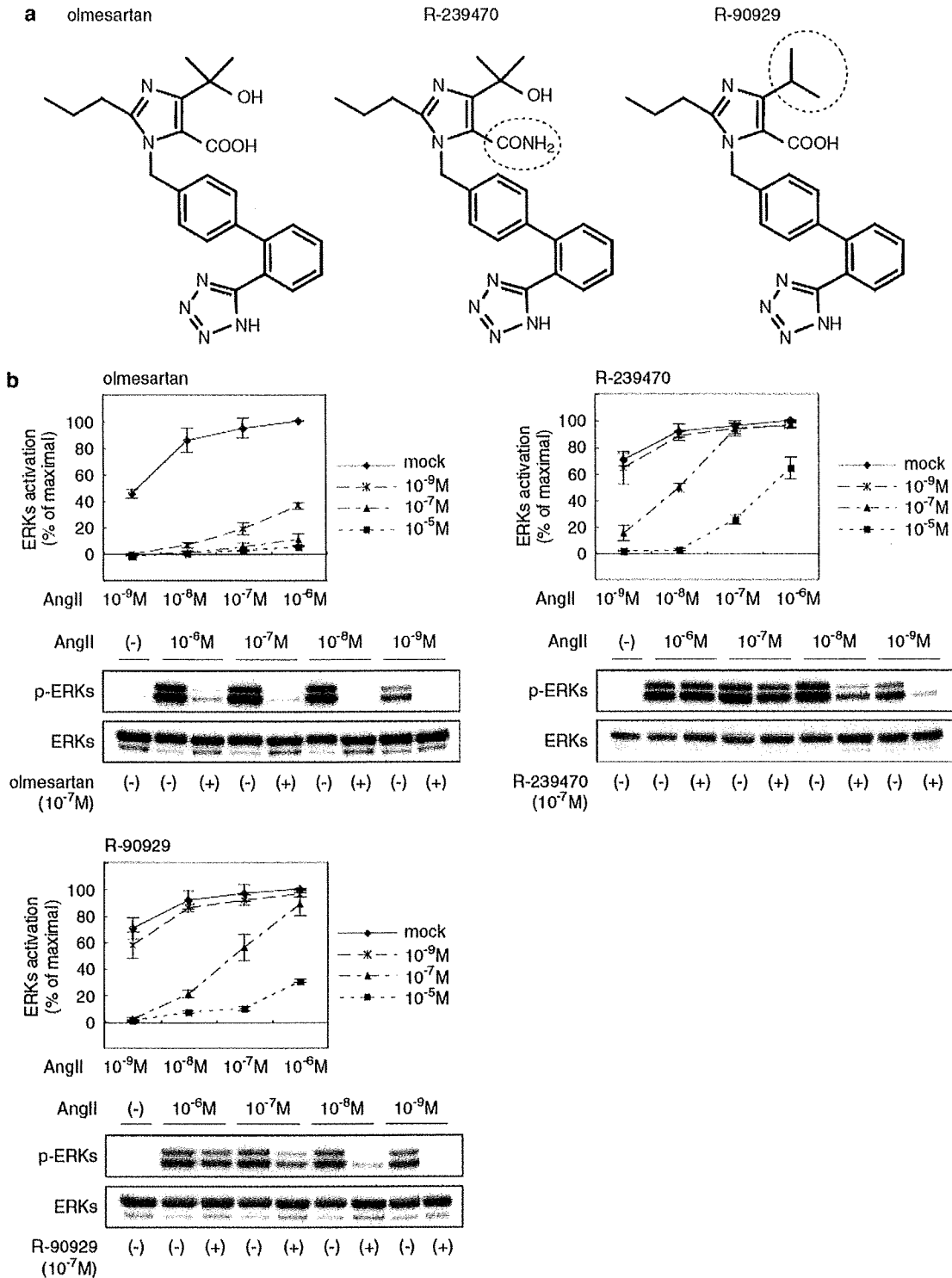
Figure 1 Continued.

during stretch-induced activation is quite different from that of the AT₁-N111G receptor.[7,10] Transmembrane domain 7 (TM7) of the AT₁ receptor undergoes a counterclockwise rotation and a shift toward the ligand-binding pocket in response to mechanical stretch,[7] but it shifts away from the ligand-binding pocket in the AT₁-N111G receptor.[10]

In this study, we show that, as an inverse agonist, olmesartan strongly inhibits the stretch-induced activation of the AT₁ receptor, as well as the constitutive activity of the AT₁-N111G receptor. In addition to the ternary interactions involving the hydroxyl group and the carboxyl group of the imidazole ring of olmesartan, a specific drug-receptor interaction between the tetrazole group of olmesartan and Gln²⁵⁷ of the AT₁ receptor is also important for the potent inverse agonist activity olmesartan exerts against stretch-induced AT₁ receptor

activation. These results provide new insights into the structure-function relationship of AT₁ receptor inverse agonists.

METHODS

Materials

Olmesartan and its derivatives (R-88145, R-90929 and R-239470) were synthesized at the Research Laboratories of Daiichi Sankyo (Tokyo, Japan). The chemical structures of these compounds are shown in Figures 1a and 6b. AngII was purchased from Sigma-Aldrich (St Louis, MO, USA).

Cell culture and transfection

Cardiomyocytes obtained from ventricles of 1-day-old Wistar rats were plated at a field density of 1×10^5 cells per cm² on collagen-coated silicone rubber

Figure 1 The carboxyl group and the hydroxyl group are critical structural characteristics of olmesartan that lead to its insurmountable inhibition of angiotensin II (AT₁) receptors. (a) The chemical structures of olmesartan and its derivative compounds, R-239470 and R-90929, are shown. Olmesartan contains a carboxyl group and a hydroxyl group on its benzimidazole ring. R-239470 has a non-acidic carbamoyl group (circled CONH₂) instead of the carboxyl group, and R-90929 has no hydroxyl group (circled). (b) Response curves of AngII-mediated extracellular signal-regulated protein kinase (ERK) activation (upper panels). HEK293-AT₁ cells were pretreated with 10^{-7} M olmesartan, R-239470 or R-90929, and stimulated by AngII at indicated concentrations (lower panels). The activation of ERKs was determined using a polyclonal antibody against phosphorylated ERKs (p-ERKs). (c) The inhibitory effects of olmesartan and its derivative compounds, R-239470 and R-90929, on AngII-induced c-fos gene expression in HEK293 cells expressing the AT₁ receptor were examined by northern blot analysis of c-fos mRNA. (d) The inhibitory effects of olmesartan and its derivative compounds, R-239470 and R-90929, on AngII-induced c-fos gene expression in HEK293 cells expressing the AT₁ receptor were examined using a luciferase assay examining c-fos promoter activation. *$P<0.01$ vs. that with no stimulation, #$P<0.01$ vs. that with AngII stimulation with no treatment, §$P<0.05$ vs. that with AngII stimulation with olmesartan (10^{-7} M) treatment.

dishes.[6] Cardiomyocytes and HEK293 cells were cultured in DMEM supplemented with 10% fetal bovine serum and nutrient-starved under serum-free conditions for 48 h before AngII or stretch stimulation. The expression vector for AT$_1$-WT and AT$_1$-mutant receptors[9] was transfected using FuGENE 6 Transfection Reagent (Roche Diagnostics, Basel, Switzerland) according to the manufacturer's instructions.[7]

Western blot analysis

Total cellular proteins (20 μg) were fractionated by SDS-PAGE and transferred to Hybond membranes (GE Healthcare, Piscataway, NJ, USA). The blotted membranes were incubated with a polyclonal antibody recognizing phospho-extracellular signal-regulated protein kinase 1/2 (ERK1/2) (Cell Signaling, Beverly, MA, USA) or ERK1/2 (Zymed Laboratories, South San Francisco, CA, USA). Horseradish peroxidase-conjugated anti-rabbit IgG (immunoglobulin G) antibody was used as secondary antibody, and signals were detected using the ECL detection kit (GE Healthcare).

RNA extraction and northern blot analysis

Total RNA was isolated from AT$_1$ receptor-transfected COS7 cells using an RNeasy Mini Kit (Qiagen, Valencia, CA, USA) according to the manufacturer's instructions, and 20 mg of total RNA was hybridized with a cDNA probe for c-fos.

Luciferase assay

The c-fos luciferase reporter plasmid, with or without the expression vector for the AT$_1$-WT or AT$_1$-N111G receptor, was transfected using FuGENE 6 Transfection Regent (Roche Diagnostics) according to the manufacturer's instructions. pRL-SV40 (Promega, Madison, WI, USA) was co-transfected as an internal control. Luciferase activity was measured 24 h after transfection using the Dual-Luciferase Reporter Assay System (Promega). Experiments were repeated at least in triplicate, and representative data are shown. The c-fos luciferase reporter plasmid was a generous gift from Dr M Tsuda (Toyama Medical and Pharmaceutical University, Toyama, Japan).

Statistical analysis

Statistical analyses comparing three or more independent experiments were carried out using one-way ANOVA (analysis of variance) and Dunnett's t-test. P-values <0.05 were considered statistically significant.

partially by pretreatment with R-239470 or R-90929 (Figure 1c). Similarly, stimulation with 10^{-6} M AngII for 24 h induced a 12-fold increase in c-fos promoter activity, which was suppressed significantly by pretreatment with olmesartan but only partially suppressed by pretreatment with R-239470 or R-90929 (Figure 1d).

Collectively, these results suggest that the carboxyl group and the hydroxyl group on the imidazole ring of olmesartan are required for
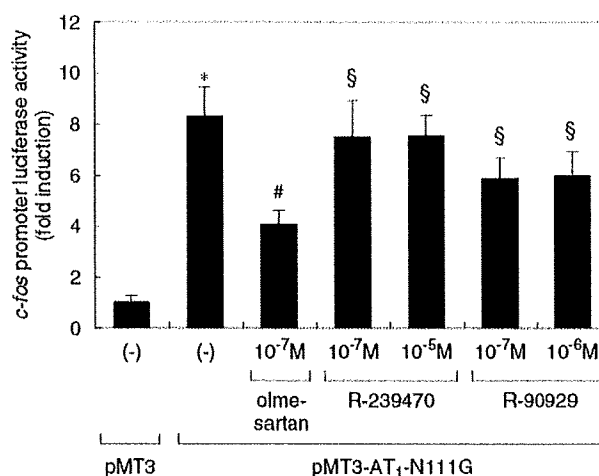

Figure 2 The carboxyl group and the hydroxyl group are critical structures in olmesartan's inverse agonist activity that allow it to suppress basal c-fos promoter activity. The basal activities of the AT$_1$-N111G mutant receptor were evaluated by a luciferase assay examining c-fos promoter activity in HEK293 cells expressing AT$_1$-N111G. Cells were treated with indicated concentrations of olmesartan, R-239470 or R-90929. *P<0.01 vs. that of pMT3-transfected cells, #P<0.01 vs. that of untreated AT$_1$-N111G-transfected cells, §P<0.05 vs. that of AT$_1$-N111G-transfected cells treated with olmesartan (10^{-7} M). AT$_1$, angiotensin II type 1.

RESULTS

Inhibitory effects of olmesartan and its derivative compounds on AngII-induced activation of the AT$_1$ receptor

We first determined the inhibitory effects of olmesartan and its derivative compounds, namely R-239470 and R-90929 (Figure 1a), on AngII-induced ERK activation. As previously reported, stimulation with AngII for 8 min induced a significant increase in the phosphorylation level of ERKs in HEK293 cells expressing the AT$_1$ receptor (Figure 1b).[7] Pretreatment with 10^{-7} M olmesartan strongly inhibited ERK activation induced even by 10^{-6} M AngII. The concentration–response curve of AngII-induced ERK activation in the presence of olmesartan (10^{-6} to 10^{-9} M) showed that olmesartan produced an insurmountable inhibitory effect on the AT$_1$ receptor, because it decreased the maximal response to AngII (Figure 1b). In contrast, R-239470 and R-90929, which lack the carboxyl or hydroxyl group possessed by olmesartan, respectively, showed surmountable inhibitory effects and led to a rightward shift of the concentration–response curve rather than a decrease in maximal response (Figure 1b).

We have further confirmed that these side-chain structures are crucial for the insurmountable inhibitory effect olmesartan exerts on AngII-induced c-fos gene expression. Stimulation with 10^{-6} M AngII significantly increased the expression level of c-fos mRNA, which was suppressed significantly by pretreatment with olmesartan but only
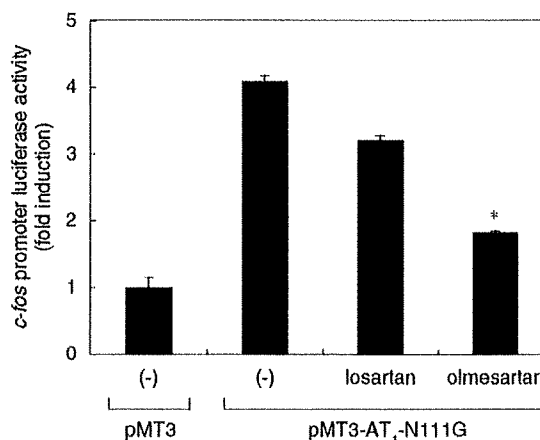

Figure 3 Comparison of the inverse agonist activities of olmesartan and losartan and their ability to suppress basal c-fos promoter activity. The basal activities of the AT$_1$-N111G mutant receptor were evaluated by a luciferase assay examining c-fos promoter activity in HEK293 cells expressing AT$_1$-N111G. The inhibitory effect of 10^{-7} M of olmesartan on basal c-fos promoter activity was much stronger than the inhibitory effect exerted by 10^{-7} M losartan. *P<0.01 vs. that of losartan. AT$_1$, angiotensin II type 1.
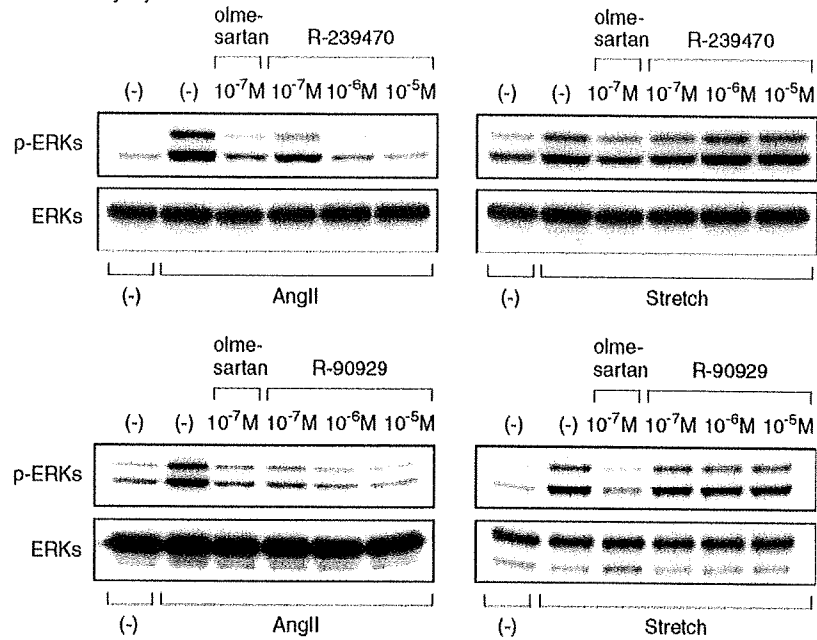
5

the insurmountable inhibition of AngII-induced activation of the AT₁ receptor.

Inhibitory effects of olmesartan and its derivative compounds on stretch-induced ERK activation

A recent study showed that olmesartan suppresses the basal production of inositol phosphate (IP) in cells expressing WT AT₁ receptor (AT₁-

WT) and a constitutively active mutant AT₁ receptor (AT₁-N111G).[9] We also found that basal c-fos promoter activity was suppressed by olmesartan in HEK293 cells expressing AT₁-N111G (Figure 2). The inhibitory effect of olmesartan on basal c-fos promoter activity was significantly stronger than that of losartan (Figure 3). Olmesartan is therefore defined as an inverse agonist of the AT₁ receptor because it decreases the basal activity level of the receptor in the absence of the agonist.
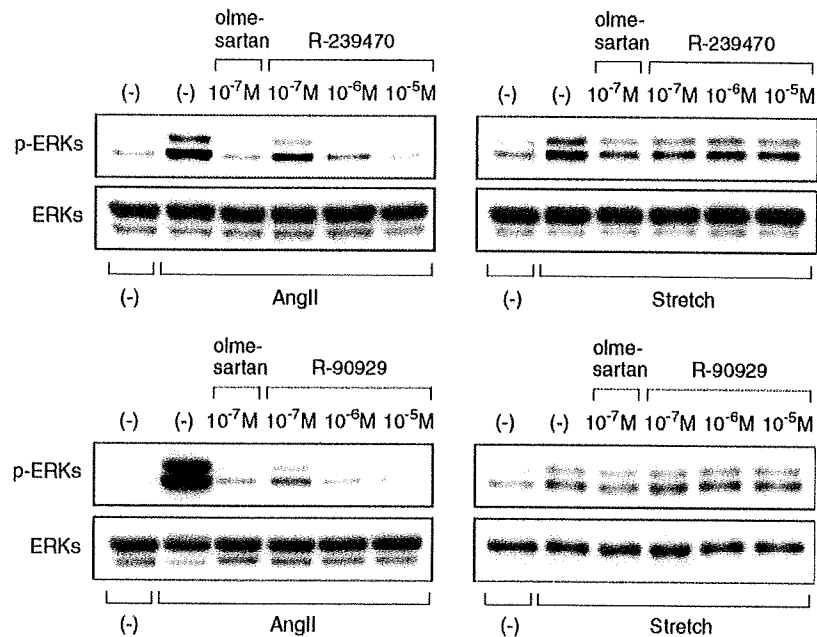

Figure 4 The carboxyl group and the hydroxyl group as critical structures for olmesartan's inverse agonist activity against stretch-induced ERK activation. Rat neonatal cardiomyocytes (a) or HEK293-AT₁ cells (b) were pretreated with indicated concentrations of olmesartan, R-239470 or R-90929, and stimulated by 10⁻⁷ M AngII (left) or by mechanical stretch (right). The activation of extracellular signal-regulated protein kinase (ERKs) was then determined. AT₁, angiotensin II type 1.

We recently reported that mechanical stress activates the AT_1 receptor independently of AngII and that this AngII-independent activation of AT_1 receptor is inhibited by the inverse agonist, candesartan.[6] Therefore, we next examined the inhibitory effects of olmesartan on stretch-induced ERK activation in cardiomyocytes cultured from neonatal rats. We found that the stretch-induced phosphorylation of ERKs in cultured cardiomyocytes was largely dependent on the direct activation of AT_1 receptor and that AngII, even if secreted from cardiomyocytes, had only a marginal role in the stretch-induced activation of ERKs.[6] We found that the activation of ERKs in response to mechanical stretch was significantly attenuated by a pretreatment with 10^{-7} M olmesartan (Figure 4a). Furthermore, to exclude the effect of secreted AngII on stretch-induced ERK activation, we imposed stretch stimulation on HEK293 cells that showed no detectable expression of angiotensinogen.[6] Neither stimulation with AngII nor mechanical stretch activated ERKs in HEK293 cells, but mechanical stretching did activate ERKs in these cells when the AT_1 receptor was overexpressed[6] (Figure 4b). Similar to the results in cardiomyocytes, pretreatment with olmesartan significantly inhibited stretch-induced ERK activation in HEK293 cells expressing the AT_1 receptor (HEK293-AT_1 cells) (Figure 4b). Furthermore, the inhibitory effect of olmesartan on stretch-induced ERK activation was significantly stronger than that of losartan (Figure 5). These results suggest that olmesartan, as a potent inverse agonist, strongly suppresses stretch-induced ERK activation, as well as the basal activity of the AT_1 receptor.

We further examined the inhibitory effects of R-239470 and R-90929 on stretch-induced ERK activation, both in cardiomyocytes and in HEK293-AT_1 cells. As shown in Figure 4, 10^{-7} M R-239470 or

R-90929 could not inhibit ERK activation induced either by 10^{-7} M AngII or by mechanical stretch, although 10^{-7} M olmesartan inhibited ERK activation. Interestingly, AngII-induced ERK activation was inhibited by 10^{-5} M R-239470 and 10^{-6} M R-90929, but stretch-induced ERK activation was not inhibited by the same concentrations of these compounds (Figure 4). These results suggest that the carboxyl and the hydroxyl groups present in olmesartan are responsible for the potent inverse agonist activity olmesartan exerts against stretch-induced ERK activation. Similar to the results of experiments evaluating stretch-induced ERK activation, 10^{-5} M R-239470 and 10^{-6} M R-90929 failed to suppress basal c-fos promoter activity in HEK293 cells expressing AT_1-N111G (Figure 2).

Inhibitory effects of olmesartan on stretch-induced ERK activation in mutated AT_1 receptors

Structure–function analyses have shown that ternary interactions between the hydroxyl group of olmesartan and Tyr^{113} of the AT_1 receptor and between the carboxyl group of olmesartan and Lys^{199} and His^{256} of the AT_1 receptor are essential for the inverse agonist activity that olmesartan exerts on basal IP production in both AT_1-WT and AT_1-N111G receptors.[9] The tetrazole group of olmesartan also interacts with Gln^{257} of the AT_1 receptor, but its binding is not required to reduce the basal activity level of the AT_1 receptor.[9] We first examined the effect of olmesartan on stretch-induced ERK activation in HEK293 cells overexpressing AT_1-WT or an AT_1 mutant receptor harboring one of the following mutations: Y113F, K199Q, H256A or Q257A. As shown in Figure 6a, mechanical stretch-induced phosphorylation of ERKs occurred in AT_1-Y113F, AT_1-K199Q, AT_1-H256A and AT_1-Q257A cells in degrees equivalent to AT_1-WT cells. Interestingly, the inhibitory effects of olmesartan on stretch-induced ERK activation were abolished in cells expressing AT_1-Y113F, AT_1-K199Q, AT_1-H256A or AT_1-Q257A (Figure 6a). These results suggest that the interactions between olmesartan and Gln^{257}, Tyr^{113}, Lys^{199} and His^{256} are required for the potent inverse agonism olmesartan exerts on stretch-induced activation of the AT_1 receptor.

As the tetrazole ring of olmesartan interacts with Gln^{257} of the AT_1 receptor,[9] we next examined the inhibitory effect that R-88145 (in which the tetrazole group was replaced with a carboxyl group, Figure 6b) had on stretch-induced ERK activation in HEK293 cells overexpressing AT_1-WT. Although 10^{-7} M R-88145 did not inhibit ERK activation induced by 10^{-7} M AngII, 10^{-5} M R-88145 could inhibit ERK activation to an extent equivalent to 10^{-7} M olmesartan (Figure 6c). However, stretch-induced ERK activation was not significantly inhibited by 10^{-5} M R-88145 (Figure 6c). These results suggest that the interaction between the tetrazole group of olmesartan and Gln^{257} of the AT_1 receptor is also responsible for the potent inverse agonist activity olmesartan exerts against stretch-induced ERK activation.

DISCUSSION

The ARBs share a common mode of action, namely they block AngII-mediated responses, but the antihypertensive potency of ARBs differs by drug.[2,4] Indeed, the pharmacokinetics of ARBs in human bodies, specifically factors such as bioavailability, half-life duration and route of elimination, differ considerably between different ARBs. These different degrees of efficacy possessed by ARBs are based on differences in their chemical structures, which determine their unique pharmacological properties. Insurmountable antagonism is one of the pharmacological parameters that is relevant to antihypertensive efficacy.[11] Insurmountable antagonism reflects tight binding and a slow dissociation of the drug–receptor complex. ARBs with insurmountable
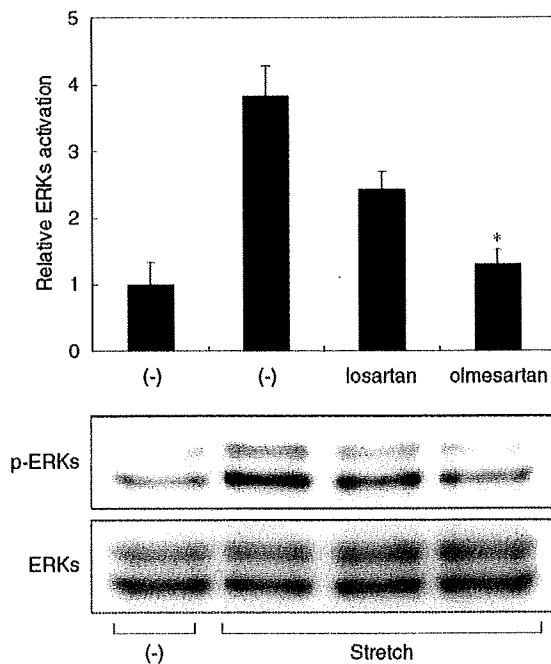

Figure 5 Comparison of the inverse agonist activities of olmesartan and losartan against stretch-induced ERK activation. HEK293-AT_1 cells were stimulated by mechanical stretch, and the activation of extracellular signal-regulated protein kinase (ERKs) was determined. The inhibitory effect of 10^{-7} M olmesartan on stretch-induced ERK activation was much stronger than that of 10^{-7} M losartan. $*P<0.01$ vs. that of losartan. AT_1, angiotensin II type 1.

antagonist properties suppress maximal AngII-induced responses.[11] Recently, it was reported that olmesartan showed a higher degree of insurmountable antagonism than did telmisartan against AngII-induced IP accumulation in CHO-K1 cells expressing the AT$_1$ receptor.[12] In this study, we showed that olmesartan shows insurmountable antagonist activity against the AT$_1$ receptor and that the carboxyl and hydroxyl groups on the imidazole ring are required for the insurmountable inhibition of AngII-induced ERK activation and c-fos gene expression (Figure 1).

The unique side-chain structure olmesartan possesses (its carboxyl group and hydroxyl group) contributes to its specific receptor-binding

activity. These drug–receptor interactions cooperate to stabilize the receptor in an inactive conformation and thereby confer inverse agonism against the basal expression of the c-fos gene (Figure 2) and the basal production of IP^9 in cells expressing the AT$_1$-N111G receptor, as well as insurmountable antagonism. The inverse agonist activities that ARBs exert against the constitutive activity of the AT$_1$ receptor could be an important pharmacological parameter that may be relevant to their efficacy at blood pressure lowering and in preventing end-organ damage. Although it remains unclear whether the subtle constitutive activity of the native AT$_1$ receptor has a pathophysiological role, the enhancement of its constitutive activity
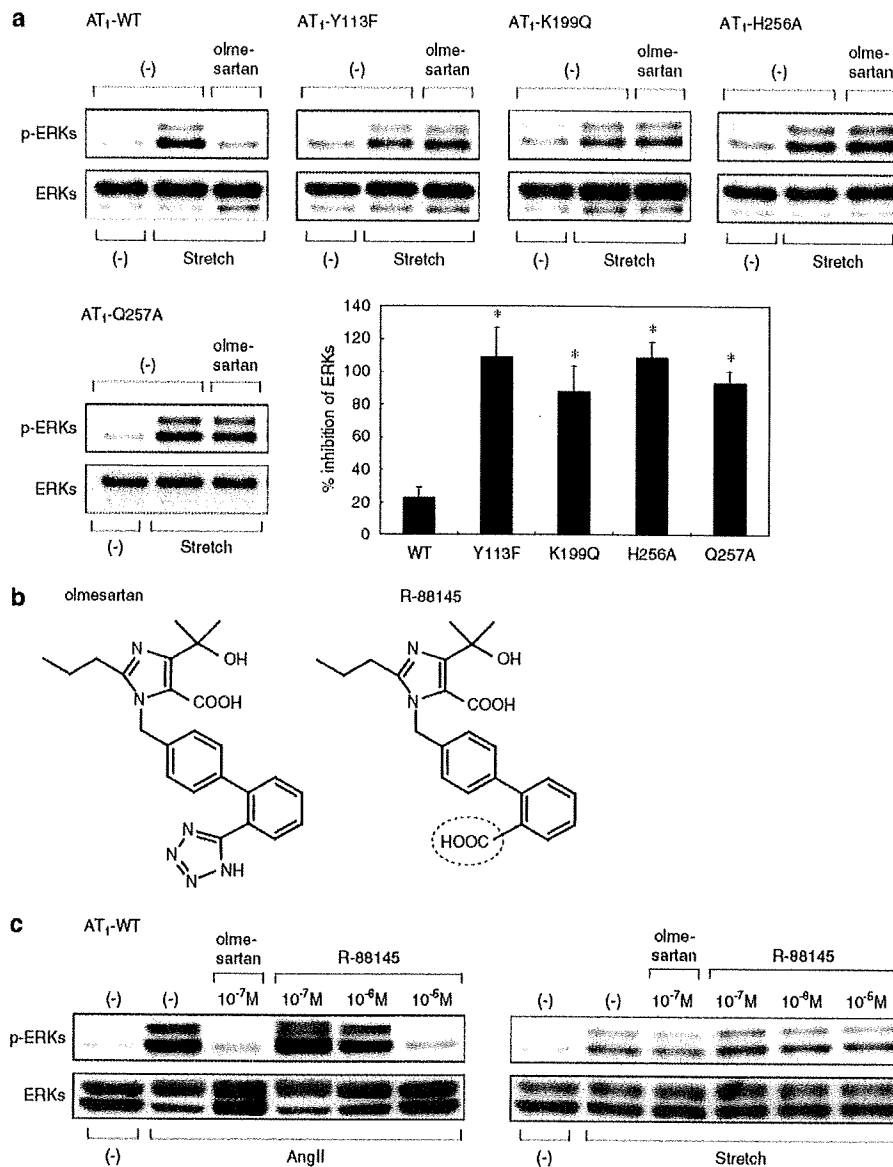

Figure 6 Specific drug–receptor interactions are required for olmesartan's inverse agonist activity against stretch-induced extracellular signal-regulated protein kinase (ERK) activation. (a) HEK293 cells expressing AT$_1$-WT, -Y113F, -K199Q, -H256A or -Q257A mutant receptors were pretreated with 10^{-7} M olmesartan and stimulated by mechanical stretch. The activation of ERKs was then determined. *P<0.01 vs. that of wild-type AT$_1$-WT. (b) The chemical structures of olmesartan and R-88145, which has a carboxyl group (circled COOH) instead of a tetrazole group. (c) HEK293-AT$_1$ cells were pretreated with indicated concentrations of olmesartan or R-88145 and were stimulated by 10^{-7} M AngII (left) or mechanical stretch (right). The activation of ERKs was then determined. AT$_1$, angiotensin II type 1.

through upregulation of receptor expression may promote cardiovascular remodeling. Indeed, the expression level of the AT_1 receptor in vascular cells is upregulated by low-density lipoprotein cholesterol,[13] insulin,[14] glucose,[15] progesterone[16] and inflammatory cytokines, such as interleukin-1α or interleukin-6.[17,18] Analyses of the binding affinity of olmesartan for mutant AT_1 receptors as well as molecular modeling analyses indicated that the ternary interactions between the hydroxyl group and Tyr[113] and between the carboxyl group and Lys[199] and His[256] are critical to the inverse agonist properties of olmesartan, but that the interaction between the tetrazole group and Gln[257] is dispensable.[9] Interestingly, differential interactions between valsartan and Ser[105], and between Ser[109] and Lys[199], are crucial for producing inverse agonism.[19] It has therefore been proposed that ARBs may bind to the AT_1 receptor primarily by docking at Lys[199] and subsequently through a distinct combination of drug–receptor interactions in a drug-specific manner.[19] According to this model, the spatial pattern of drug–receptor contact points will determine the potency of the inverse agonist activity of a given ARB.

We recently showed that mechanical stretching of cells induces a counterclockwise rotation and a shift of TM7 of the AT_1 receptor toward the ligand-binding pocket.[7] However, TM7 shifts away from the ligand-binding pocket in the AT_1-N111G receptor,[10] implying that the conformation of AT_1 receptor during stretch-induced activation is different from that of the constitutively active AT_1 receptor. In general, GPCRs are structurally flexible and unstable, and multiple conformational states exist during the GPCR activation process.[20–22] In this study, we showed that, aside from the ternary drug–receptor interactions involving the hydroxyl and carboxyl groups of olmesartan, an additional interaction between the tetrazole group of olmesartan and Gln[257] of the AT_1 receptor is required for its potent inverse agonism against stretch-induced AT_1 receptor activation (Figures 4 and 6). Each of the quaternary interactions involving the hydroxyl group, carboxyl group and tetrazole group contributes to a tight drug–receptor binding,[9] but is not sufficient enough to produce a potent inverse agonism against stretch-induced AT_1 receptor activation. Thus, the quaternary drug–receptor interactions work together to stabilize the receptor in an inactive conformation, even under conditions in which mechanical stretching occurs.

With regard to candesartan, the carboxyl group on the benzimidazole ring is responsible for its inverse agonism and leads to the suppression of both the constitutive activity and the mechanical stress-induced activation of the AT_1 receptor.[7] The SCAM studies showed that the binding of the carboxyl group of candesartan to Gln[257] of TM6 and Thr[287] of TM7 forcibly induces a clockwise rotation of TM6 and TM7, and leads to the stabilization of the AT_1 receptor in an inactive conformation.[7] At present, it remains unclear how the helical movement of TM7 induced by mechanical stretch is affected by the presence of olmesartan. According to molecular modeling, Thr[287] of TM7 is located in a position that would allow it to form a hydrogen bond with His[256] of TM6.[9] We assume that the helical movements of TM6 and TM7 are coupled and that TM7 may be restricted in motion when TM6 is rigidly bound to olmesartan through the dual interactions between the carboxyl group and His[256] and between the tetrazole group of olmesartan and Gln[257].

Our study shows that olmesartan strongly inhibits both AngII-dependent and AngII-independent activation of the AT_1 receptor. Ternary drug–receptor interactions between the hydroxyl group and Tyr[113] and between the carboxyl group and Lys[199] and His[256] are crucial for olmesartan's inverse agonist activity against the constitutive activity of an AT_1 mutant receptor, AT_1-N111G. In addition, a drug–receptor interaction between the tetrazole group of olmesartan and

Gln[257] of the AT_1 receptor is required for potent inverse agonism against stretch-induced AT_1 receptor activation. These results suggest that multivalent drug–receptor interactions cooperate in combination to stabilize the receptor in an inactive conformation according to the distinct processes of receptor activation. The inverse agonist activity of ARBs has therapeutic benefits in the prevention of load-induced cardiac hypertrophy,[5] and thus has the potential to affect long-term outcomes in patients with hypertension. Elucidation of the molecular basis for the inverse agonist activity of ARBs in relation to their chemical structure will help to categorize ARBs according to their individual efficacies in receptor inactivation and will also help researchers to develop novel ARBs with superb efficacy in terms of blood pressure lowering and end-organ protection.

CONFLICT OF INTEREST

The authors declare no conflict of interest.

ACKNOWLEDGEMENTS

1 de Gasparo M, Catt KJ, Inagami T, Wright JW, Unger T. International union of pharmacology. XXIII. The angiotensin II receptors. *Pharmacol Rev* 2000; 52: 415–472.
2 Zaman MA, Oparil S, Calhoun DA. Drugs targeting the renin-angiotensin-aldosterone system. *Nat Rev Drug Discov* 2002; 1: 621–636.
3 Kjeldsen SE, Dahlof B, Devereux RB, Julius S, Aurup P, Edelman J, Beevers G, de Faire U, Fyhrquist F, Ibsen H, Kristianson K, Lederballe-Pedersen O, Lindholm LH, Nieminen MS, Omvik P, Oparil S, Snapinn S, Wedel H. Effects of losartan on cardiovascular morbidity and mortality in patients with isolated systolic hypertension and left ventricular hypertrophy: a Losartan Intervention for Endpoint Reduction (LIFE) substudy. *JAMA* 2002; 288: 1491–1498.
4 Oparil S. Newly emerging pharmacologic differences in angiotensin II receptor blockers. *Am J Hypertens* 2000; 13: 18S–24S.
5 Akazawa H, Yasuda N, Komuro I. Mechanisms and functions of agonist-independent activation in the angiotensin II type 1 receptor. *Mol Cell Endocrinol* 2009; 302: 140–147.
6 Zou Y, Akazawa H, Qin Y, Sano M, Takano H, Minamino T, Makita N, Iwanaga K, Zhu W, Kudoh S, Toko H, Tamura K, Kihara M, Nagai T, Fukamizu A, Umemura S, Iiri T, Fujita T, Komuro I. Mechanical stress activates angiotensin II type 1 receptor without the involvement of angiotensin II. *Nat Cell Biol* 2004; 6: 499–506.
7 Yasuda N, Miura S, Akazawa H, Tanaka T, Qin Y, Kiya Y, Imaizumi S, Fujino M, Ito K, Zou Y, Fukuhara S, Kunimoto S, Fukuzaki K, Sato T, Ge J, Mochizuki N, Nakaya H, Saku K, Komuro I. Conformational switch of angiotensin II type 1 receptor underlying mechanical stress-induced activation. *EMBO Rep* 2008; 9: 179–186.
8 Milligan G. Constitutive activity and inverse agonists of G protein-coupled receptors: a current perspective. *Mol Pharmacol* 2003; 64: 1271–1276.
9 Miura S, Fujino M, Hanzawa H, Kiya Y, Imaizumi S, Matsuo Y, Tomita S, Uehara Y, Karnik SS, Yanagisawa H, Koike H, Komuro I, Saku K. Molecular mechanism underlying inverse agonist of angiotensin II type 1 receptor. *J Biol Chem* 2006; 281: 19288–19295.
10 Boucard AA, Roy M, Beaulieu ME, Lavigne P, Escher E, Guillemette G, Leduc R. Constitutive activation of the angiotensin II type 1 receptor alters the spatial proximity of transmembrane 7 to the ligand-binding pocket. *J Biol Chem* 2003; 278: 36628–36636.
11 Van Liefde I, Vauquelin G. Sartan-AT(1) receptor interactions: in vitro evidence for insurmountable antagonism and inverse agonism. *Mol Cell Endocrinol* 2009; 302: 237–243.
12 Le MT, Pugsley MK, Vauquelin G, Van Liefde I. Molecular characterisation of the interactions between olmesartan and telmisartan and the human angiotensin II AT1 receptor. *Br J Pharmacol* 2007; 151: 952–962.
13 Nickenig G, Jung O, Strehlow K, Zolk O, Linz W, Scholkens BA, Bohm M. Hypercholesterolemia is associated with enhanced angiotensin AT1-receptor expression. *Am J Physiol* 1997; 272: H2701–H2707.

14 Nickenig G, Roling J, Strehlow K, Schnabel P, Bohm M. Insulin induces upregulation of vascular AT1 receptor gene expression by posttranscriptional mechanisms. *Circulation* 1998; 98: 2453–2460.

15 Sodhi CP, Kanwar YS, Sahai A. Hypoxia and high glucose upregulate AT1 receptor expression and potentiate ANG II-induced proliferation in VSM cells. *Am J Physiol Heart Circ Physiol* 2003; 284: H846–H852.

16 Nickenig G, Strehlow K, Wassmann S, Baumer AT, Albory K, Sauer H, Bohm M. Differential effects of estrogen and progesterone on AT(1) receptor gene expression in vascular smooth muscle cells. *Circulation* 2000; 102: 1828–1833.

17 Sasamura H, Nakazato Y, Hayashida T, Kitamura Y, Hayashi M, Saruta T. Regulation of vascular type 1 angiotensin receptors by cytokines. *Hypertension* 1997; 30: 35–41.

18 Wassmann S, Stumpf M, Strehlow K, Schmid A, Schieffer B, Bohm M, Nickenig G. Interleukin-6 induces oxidative stress and endothelial dysfunction by overexpression of the angiotensin II type 1 receptor. *Circ Res* 2004; 94: 534–541.

19 Miura S, Kiya Y, Kanazawa T, Imaizumi S, Fujino M, Matsuo Y, Karnik SS, Saku K. Differential bonding interactions of inverse agonists of angiotensin II type 1 receptor in stabilizing the inactive state. *Mol Endocrinol* 2008; 22: 139–146.

20 Gether U. Uncovering molecular mechanisms involved in activation of G protein-coupled receptors. *Endocr Rev* 2000; 21: 90–113.

21 Miura S, Saku K, Karnik SS. Molecular analysis of the structure and function of the angiotensin II type 1 receptor. *Hypertens Res* 2003; 26: 937–943.

22 Perez DM, Karnik SS. Multiple signaling states of G-protein-coupled receptors. *Pharmacol Rev* 2005; 57: 147–161.
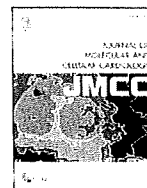
Original article

Chronic doxorubicin cardiotoxicity is mediated by oxidative DNA damage-ATM-p53-apoptosis pathway and attenuated by pitavastatin through the inhibition of Rac1 activity

Masashi Yoshida [a], Ichiro Shiojima [a,b], Hiroyuki Ikeda [a], Issei Komuro [a,b,*]

[a] Department of Cardiovascular Science and Medicine, Chiba University Graduate School of Medicine, 1-8-1 Inohana, Chuo-ku, Chiba, 260-8670, Japan
[b] Department of Cardiovascular Medicine, Osaka University Graduate School of Medicine, 2-2 Yamadaoka, Suita 565-0871, Japan

ARTICLE INFO

ABSTRACT

Doxorubicin is known to have cumulative dose-dependent cardiotoxicity, and a tumor suppressor protein p53 has been implicated in the pathogenesis of doxorubicin cardiotoxicity. However, how p53 is induced by doxorubicin and mediates the cardiotoxic effects of doxorubicin remains elusive. In cultured cardiac myocytes, doxorubicin induced oxidative stress, DNA damage, ATM activation, and p53 induction. A free radical scavenger NAC attenuated all of these events, whereas an ATM kinase inhibitor wortmannin attenuated doxorubicin-induced ATM activation and p53 induction but not oxidative stress. Doxorubicin treatment in vivo also induced oxidative stress, DNA damage, ATM activation, and p53 accumulation. These observations suggest that p53 induction by doxorubicin is mediated by oxidative DNA damage-ATM pathway. Doxorubicin-induced contractile dysfunction and myocyte apoptosis in vivo were attenuated in heterozygous p53 deficient mice and cardiac-restricted Bcl-2 transgenic mice, suggesting that myocyte apoptosis plays a central role downstream of p53 in doxorubicin cardiotoxicity. We also tested whether pitavastatin exerts protective effects on doxorubicin cardiotoxicity. Pitavastatin attenuated doxorubicin-induced oxidative stress, DNA damage, ATM activation, p53 accumulation, and apoptosis in vitro. Pitavastatin also attenuated myocyte apoptosis and contractile dysfunction in vivo. The beneficial effects of pitavastatin were reversed by intermediate products of the mevalonate pathway that are required for the activation of Rac1, and Rac1 inhibitor exhibited cardioprotective effects comparable to those of pitavastatin. These data collectively suggest that doxorubicin-induced cardiotoxicity is mediated by oxidative DNA damage-ATM-p53-apoptosis pathway, and is attenuated by pitavastatin through its antioxidant effect involving Rac1 inhibition.

1. Introduction

Doxorubicin is a potent chemotherapeutic agent used for a wide variety of malignancies. However, the use of doxorubicin is limited due to its cumulative dose-dependent cardiotoxicity, which some-times results in doxorubicin cardiomyopathy [1,2]. Although the precise mechanism of doxorubicin-induced cardiotoxicity is not completely understood, oxidative stress has been proposed as one of the mechanisms of cardiotoxicity by doxorubicin. Acute or chronic doxorubicin cardiotoxicity is reduced in transgenic mice overexpres-sing mitochondrial MnSOD or cysteine-rich metallothioneins, respec-tively [3,4], supporting the idea that oxidative stress mediates doxorubicin cardiotoxicity. It has also been suggested that a tumor suppressor protein p53 is a critical mediator of doxorubicin cardiotoxicity. This notion is supported by the observation that

doxorubicin induces p53 accumulation in the heart and that either pharmacological or genetic ablation of p53 results in the attenuation of cardiotoxicity following doxorubicin treatment [5,6]. However, how p53 is activated in the heart by doxorubicin or how p53 mediates the cardiotoxic effects of doxorubicin remains elusive. Although myocyte apoptosis induced by doxorubicin was attenuated by p53 ablation [5,6], this does not directly demonstrate the causative role of cardiomyocyte apoptosis in doxorubicin-mediated cardiotoxicity. It was recently shown that p53 inhibits hypoxia-inducible factor-1 (Hif-1) and thereby promotes myocardial ischemia [7]. More recently, p53-dependent inhibition of mammalian target of rapamycin (mTOR) was proposed as a mechanism of acute doxorubicin cardiotoxicity independently of p53-induced apoptosis [8]. Thus, it is possible that p53-dependent but apoptosis-independent mechanisms also contrib-ute to the pathogenesis of doxorubicin cardiotoxicity.

The 3-hydroxy-3-methylglutaryl-CoA (HMG-CoA) reductase inhibi-tors or statins are widely used as a cholesterol lowering drug, and also known to be cardioprotective through lipid lowering-independent pleiotropic effects [9]. For instance, statin treatment protects against

* Corresponding author. Department of Cardiovascular Science and Medicine, Chiba University Graduate School of Medicine, 1-8-1 Inohana, Chuo-ku, Chiba, 260-8670, Japan.
E-mail address: komuro-tky@umin.ac.jp (I. Komuro).

stroke, ischemia–reperfusion injury, cardiac hypertrophy, and heart failure in normocholesterolemic animals [10–13]. Most of these pleiotropic effects are thought to be mediated by inhibiting the synthesis of isoprenoid intermediates such as farnesyl pyrophosphate (FPP) and geranylgeranyl pyrophosphate (GGPP) downstream of the mevalonate pathway [9]. FPP and GGPP serve as lipid attachments for the post-translational modifications of a variety of proteins including small G proteins. Of note, activation of NADPH oxidase requires geranylgeranylation of Rac1 [14], and it was shown that the protective effect of statins against cardiac hypertrophy is mediated by its antioxidant effects involving the inhibition of Rac1 activity [12]. Whether statins exert protective effects against doxorubicin cardiotoxicity by similar mechanisms remains unknown.

In this study we explored how p53 accumulation is induced by doxorubicin and how p53 mediates the cardiotoxic effects of doxorubicin. We also examined the potential mechanisms of cardioprotection by statins against doxorubicin. We show that doxorubicin cardiotoxicity is mediated by oxidative DNA damage-ATM-p53-apoptosis pathway and attenuated by pitavastatin through the inhibition of Rac1 activity.

2. Materials and methods

2.1. Reagents

Doxorubicin was from Kyowa Hakko Kogyo (Tokyo, Japan). N-acetyl-L-cysteine (NAC), mevalonolactone, farnesyl pyrophosphate (FPP), geranylgeranyl pyrophosphate (GGPP), NADPH, and lucigenin were from Sigma (St. Louis, Missouri). Wortmannin, farnesyltransferase inhibitor (FTI (FTI-276)), geranylgeranyl transferase inhibitor (GTI (GTI-286)), Rac1 inhibitor (NSC23766), and apocynin were from Calbiochem (San Diego, California). Dihydroethidium (DHE) and 5-(and-6)-chloromethyl-2′, 7′-dichlorodihydrofluorescein diacetate, acetyl ester (CM-H2DCFDA) were from Molecular Probes (Eugene, Oregon). Hydrogen peroxide (H_2O_2) was from Wako (Osaka, Japan). Pitavastatin was provided by Kowa (Tokyo, Japan).

2.2. Cell culture and treatment

Neonatal rat cardiomyocytes were prepared as previously described [15]. Doxorubicin (1 μM) was added to culture media 24 h after myocyte preparation. Where indicated, cells were pretreated for 30 min with the following compounds: wortmannin, 1–50 μM; NAC, 1–50 μM; pitavastatin, 0.1–10 μM; mevalonate, 200 μM; GGPP, 10 μM; FPP, 10 μM; GTI, 30 μM; FTI, 20 nM; Rac1 inhibitor, 100 μM.

2.3. Animal models

C57BL/6 mice were purchased from SLC (Shizuoka, Japan). Heterozygous p53 deficient mice on C57BL/6 background were from Jackson Laboratory (Bar Harbar, Maine). For experiments using p53 heterozygous knockout mice, C57BL/6 mice were used as controls. Generation and genotyping of transgenic mice with cardiac-restricted overexpression of human Bcl-2 have been previously described [16]. Bcl-2 transgenic mice were on mixed background and their non-transgenic littermates were used as controls. Doxorubicin treatment was performed with intraperitoneal injection of doxorubicin (6 mg/kg) once a week for 4 weeks. Pitavastatin (3 mg/kg) treatment was performed with daily oral administration. All animal procedures were performed with the approval of the Institutional Animal Care and Use Committee of Chiba University.

2.4. Echocardiography

Transthoracic echocardiography was performed with Vevo 660 (VISUAL SONIC, Ontario, Canada) equipped with a 25-MHz imaging transducer. All recordings were performed on conscious animals.

2.5. Oxidative stress detection

Total intracellular oxidation in cultured cardiomyocytes was assessed with 2′, 7′-dichlorofluorescein (DCF) fluorescence using CM-H2DCFDA. Intracellular oxidative stress was monitored by microscopic observation and measurement of intracellular fluorescence intensity using the Mithras LB940 (Berthold, Germany) as previously described [17]. Measurements were carried out for 5 samples in each group according to the manufacturer's instruction. Histological detection of superoxide production was assessed with DHE as previously described [18].

2.6. DNA damage detection

To assess DNA damage in cultured cardiomyocytes, CometAssay (Trevigen, Gaithersburg, MD, USA) was performed according to the manufacturer's instruction. During electrophoresis, undamaged DNA remains within the confines of the nucleus, whereas damaged DNA migrates out of the nucleus in the shape of a comet. Each comet was assigned a value of 0 (no tail) to 4 (almost all DNA in tail), and 100 cells per slide and 3 slides per treatment were analyzed. To assess DNA damage in the heart in vivo, paraffin sections of the heart samples fixed in 10% formalin were stained with an antibody against phosphorylated histone H2AX (γH2AX) (Cell Signaling Technology, Beverly, Massachusetts) and dystrophin (Novocastra Laboratories, Newcastle, UK).

2.7. Western blot analysis

Western blot analysis was performed as previously described [7]. Unless mentioned otherwise, whole cell or tissue lysates were used for analysis. For Rac1 subcellular localization assay, membrane and cytosolic proteins were prepared using proteoextract native membrane protein extraction kit (Calbiochem) according to the manufacturer's instruction. Specific signals were detected using enhanced chemiluminescence (Amersham, Buckinghamshire, UK). The primary antibodies used for western blotting were as follows: phospho-ATM (S1981) (Rockland, Philadelphia, Pennsylvania), ATM (Santa Cruz Biotechnology), phospho-p53 (S15) (Santa Cruz Biotechnology), p53 (Cell Signaling Technology), Bax (Santa Cruz Biotechnology), cleaved caspase-3 (Cell Signaling Technology), Rac1 (Santa Cruz Biotechnology), and actin (Sigma).

2.8. NADPH oxidase assay

NADPH oxidase activity was measured as previously described [19]. All measurements were performed as triplicates in 96-well luminometer plates.

2.9. Cell death assay

The number of viable cells in vitro was determined with trypan blue exclusion method [20]. For apoptosis analysis in vitro and in vivo, TUNEL labeling was performed according to the manufacturer's protocol (In Situ Apoptosis Detection Kit; Takara, Shiga, Japan). TUNEL-positive cells were counted in 3 randomly selected low-power fields from each culture dish, 3 dishes for each group in vitro. TUNEL/dystrophin double positive cells were counted in 20 randomly selected high-power fields from each heart sample in vivo.

2.10. Statistical analysis

All values are expressed as means ± SEM. Multiple group comparison was performed by one-way ANOVA followed by the Tukey's HSD for comparison of means. Comparisons between two groups were analyzed by two-way ANOVA. Data processing and analysis were performed by using JMP version 5.1 (Statical Analysis
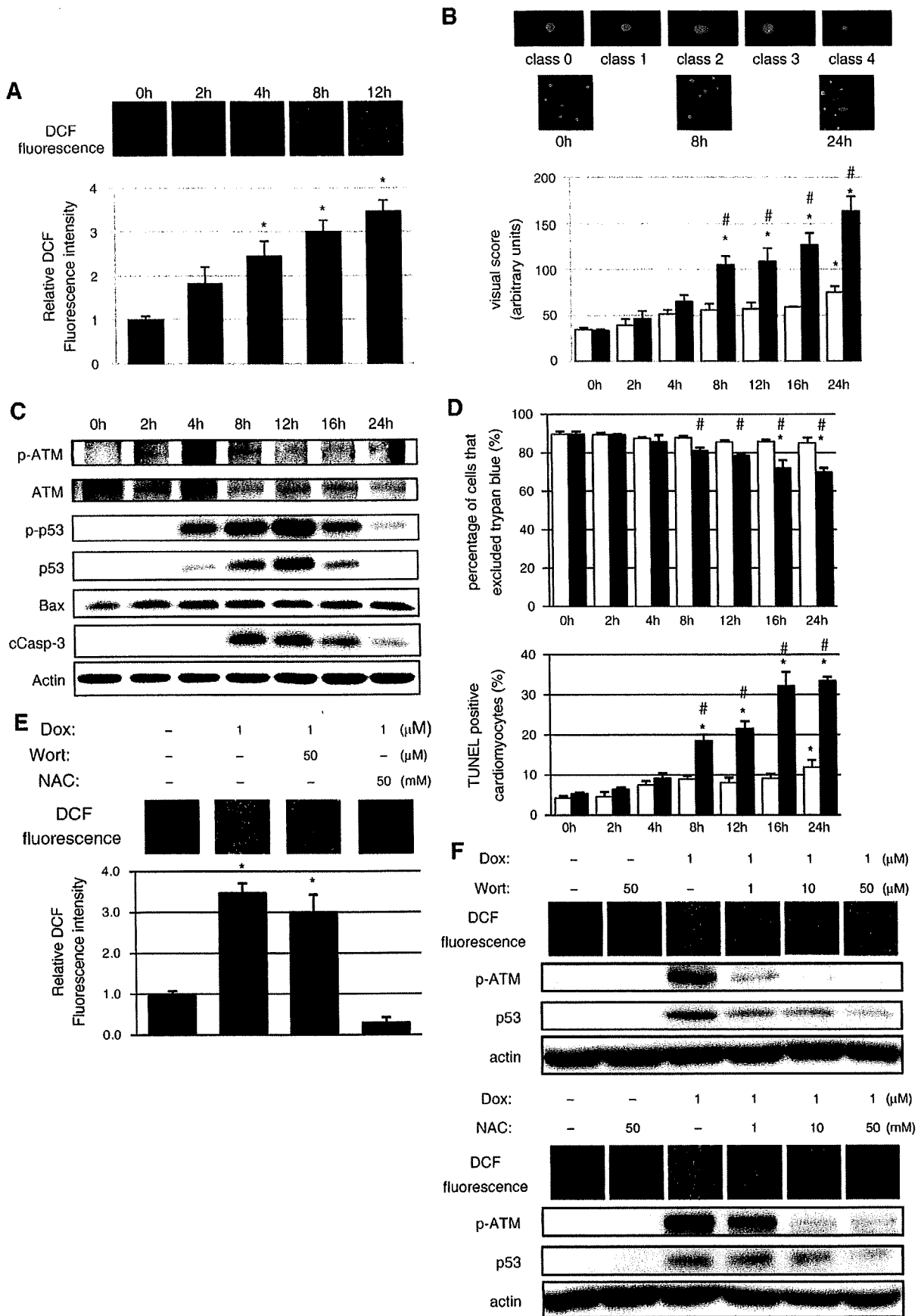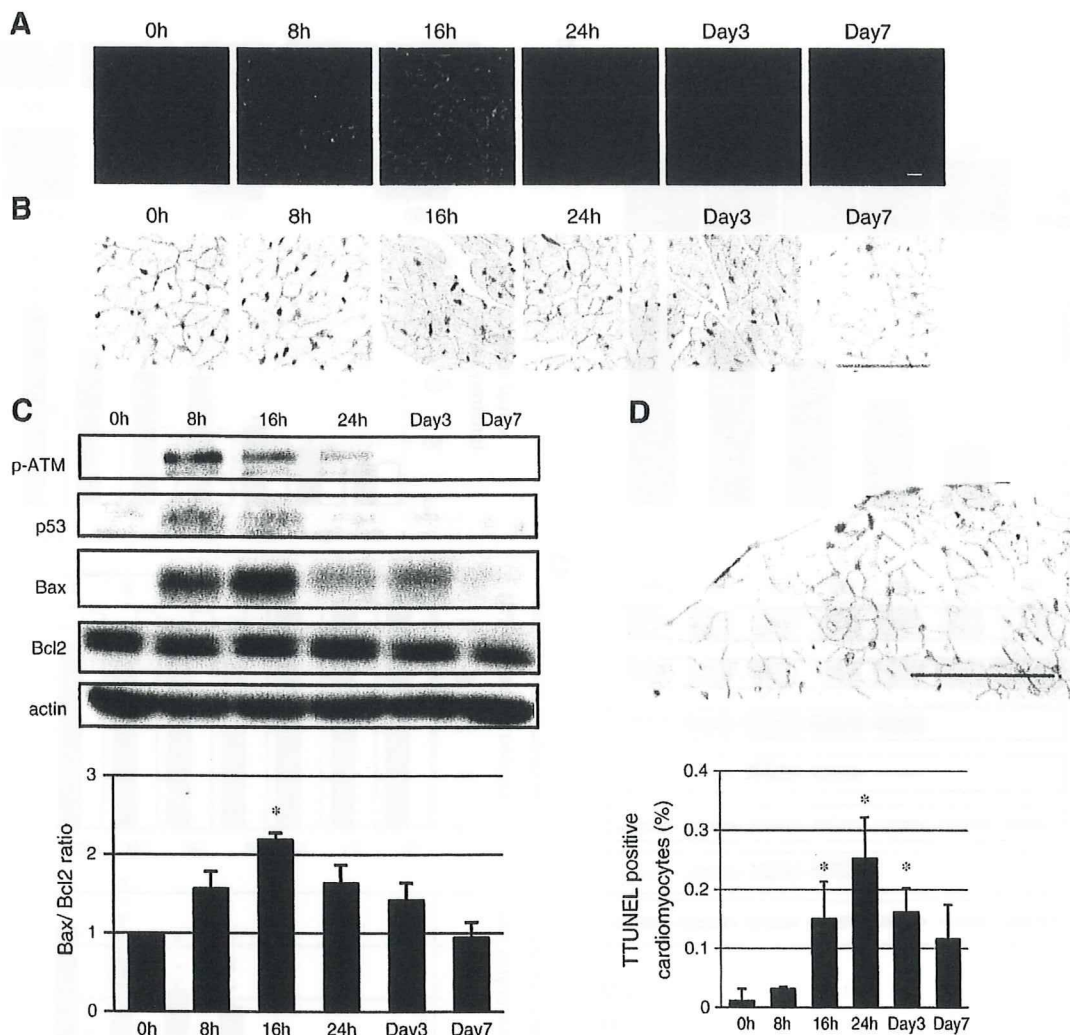
Fig. 2. Doxorubicin induces oxidative DNA damage, ATM kinase activation, and p53 accumulation in the heart in vivo. (A) Doxorubicin-induced oxidative stress in vivo. Oxidative stress was assessed by DHE assay. (B) Doxorubicin-induced DNA damage in vivo. DNA damage was assessed by γH2AX staining. (C) Doxorubicin-induced ATM activation, p53 accumulation, and cardiomyocyte apoptosis in vivo. Left: Western blot analysis. Molecular weight of Bcl2 is 26 kDa. Right: quantification of Bax/Bcl2 ratio. *$P < 0.05$ vs 0 h. (D) Doxorubicin-induced cardiomyocyte apoptosis as assessed by TUNEL staining. Left: double-immunostaining for TUNEL (brown) and dystrophin (red) in the heart after doxorubicin treatment. Scale bar, 100 μm. Right: time course of the number of TUNEL-positive cardiomyocytes. *$P < 0.05$ vs 0 h.

Systems). Values of $P < 0.05$ were considered to be statistically significant.

3. Results

3.1. Doxorubicin induces p53 accumulation in cardiac myocytes via oxidative DNA damage-ATM pathway

Previous studies implicated oxidative stress and p53 accumulation in doxorubicin cardiotoxicity [1,2]. Because DNA damage

links oxidative stress to p53 accumulation [21,22], we tested whether DNA damage response mediates doxorubicin cardiotoxicity in cultured cardiac myocytes. Doxorubicin treatment induced oxidative stress and DNA damage in cardiac myocytes, as assessed by DCF fluorescence and CometAssay. Statistically significant increase in DCF fluorescence and DNA damage was observed from 4 h and 8 h after doxorubicin treatment, respectively (Figs. 1(A) and (B)). Increased oxidative stress and DNA damage was associated with an increase in phospho-ATM (ataxia telangiectasia mutated) levels, p53 accumulation, and

Fig. 1. Doxorubicin induces p53 accumulation in cardiac myocytes through oxidative DNA damage-ATM pathway. (A) Doxorubicin-induced oxidative stress. Top: DCF fluorescence. Bottom: quantification of DCF fluorescence. *$P < 0.05$ vs 0 h. (B) Doxorubicin-induced DNA damage as assessed by CometAssay. Top: classification of comets from 0 (no tail) to 4 (almost all DNA in tail). Middle: representative pictures of CometAssay at indicated time points. Bottom: time course of visual scores. White columns and black columns represent control (saline-treated) group and doxorubicin-treated group, respectively. *$P < 0.05$ vs control group at 0 h; #$P < 0.05$ vs control group at the same time points. (C) Doxorubicin-induced ATM activation, p53 accumulation, and cardiomyocyte apoptosis as assessed by Western blot analysis. cCasp-3, cleaved caspase-3. Molecular weights of the proteins are 370 kDa for pATM/ATM, 53 kDa for p-p53/p53, 23 kDa for Bax, 19 kDa for cleaved caspase-3, and 42 kDa for actin. (D) Doxorubicin-induced cardiomyocyte death. Top: trypan blue exclusion assay. White columns and black columns represent control (saline-treated) group and doxorubicin-treated group, respectively. *$P < 0.05$ vs control group at 0 h; #$P < 0.05$ vs control group at the same time points. Bottom: TUNEL assay. White columns and black columns represent control (saline-treated) group and doxorubicin-treated group, respectively. *$P < 0.05$ vs control group at 0 h; #$P < 0.05$ vs control group at the same time points. (E) NAC but not wortmannin attenuates doxorubicin-induced oxidative stress. Top: DCF fluorescence. Bottom: quantification of DCF fluorescence. *$P < 0.05$ vs 0 h. (F) Both NAC and wortmannin attenuates doxorubicin-induced ATM activation and p53 accumulation. DCF fluorescence, ATM, and phospho-p53 were assessed 12 h, 4 h, and 12 h after doxorubicin treatment, respectively. Wort, wortmannin.

apoptotic cell death (Figs. 1(C) and (D)). Definitive increases in phospho-ATM and phospho-p53 were observed from 4 h after doxorubicin treatment, followed by cleaved Caspase-3 expression and apoptotic cell death from 8 h after doxorubicin treatment. This is consistent with the notion that p53 phosphorylation by ATM results in p53 stabilization, leading to apoptotic cell death. Doxorubicin-induced oxidative stress was attenuated by a free radical scavenger NAC but not by an ATM kinase inhibitor wortmannin, whereas doxorubicin-induced p53 accumulation was

reduced both by NAC and wortmannin (Figs. 1(E) and (F)), indicating that ATM is situated downstream of oxidative stress in doxorubicin-induced p53 accumulation. We also checked the involvement of oxidative DNA damage-ATM pathway in doxorubicin cardiotoxicity in vivo. Single intra-peritoneal injection of doxorubicin (6 mg/kg) induced oxidative stress and DNA damage as assessed by DHE assay and γH2AX staining, respectively (Figs. 2(A) and (B)). Doxorubicin-induced oxidative stress and DNA damage in the heart were associated with a transient increase in
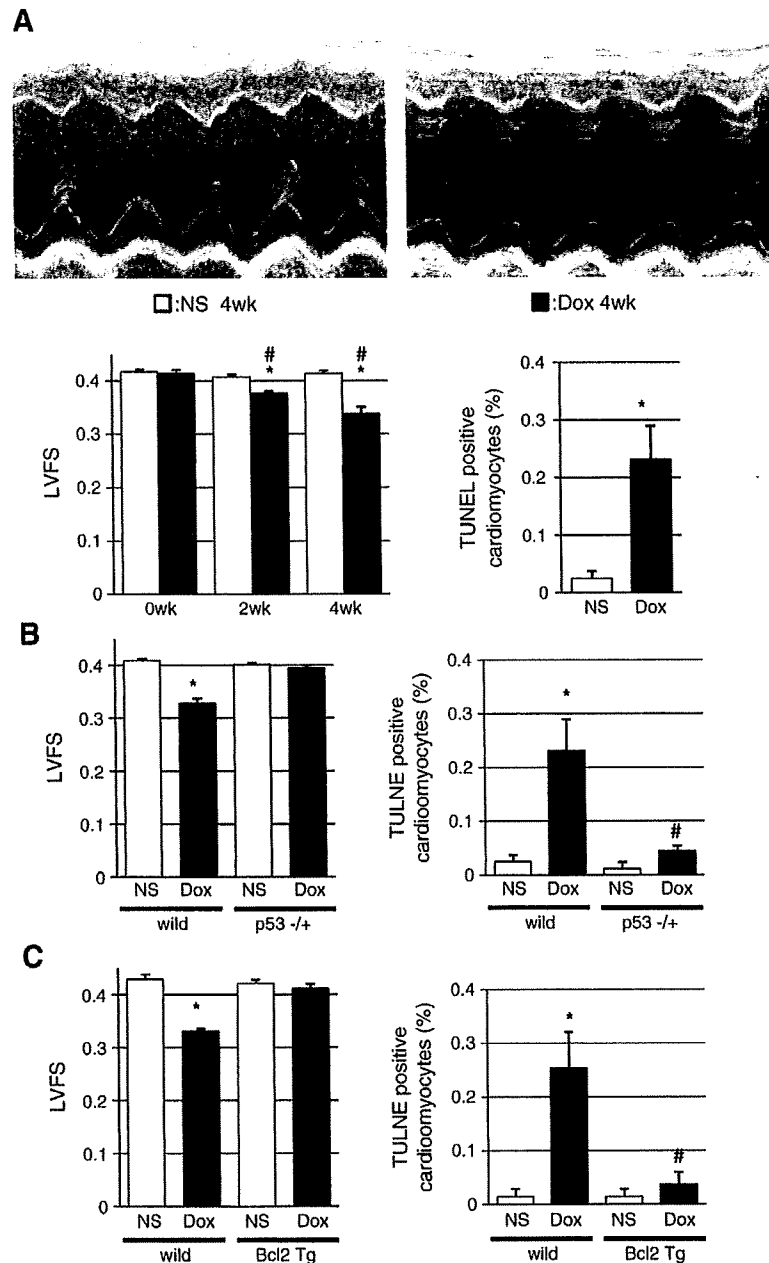

Fig. 3. Doxorubicin cardiotoxicity is mediated by p53-dependent cardiomyocyte apoptosis. (A) Doxorubicin-induced cardiomyopathy in wild type mice. Top: representative echocardiograms of the heart treated with normal saline (NS) or doxorubicin (Dox: 6 mg/kg) once a week for 4 weeks. Bottom left: left ventricular fractional shortening of mice treated with normal saline (white columns) or doxorubicin (black columns). *P<0.05 vs 0 week; #P<0.05 vs normal saline-treated group at the same time point. Bottom right: number of TUNEL-positive cardiomyocytes 4 weeks after doxorubicin treatment. *P<0.05 vs normal saline (NS)-treated group. (B) Doxorubicin-induced cardiomyopathy is attenuated in heterozygous p53 deficient mice. Left: left ventricular fractional shortening of mice treated with normal saline (NS) or doxorubicin (Dox). Right: number of TUNEL-positive cardiomyocytes 4 weeks after doxorubicin treatment. *P<0.05 vs saline-treated wild type mice; #P<0.05 vs doxorubicin-treated wild type mice. (C) Doxorubicin-induced cardiomyopathy is attenuated in cardiac-specific Bcl-2 transgenic mice. Left: left ventricular fractional shortening of mice treated with normal saline (NS) or doxorubicin (Dox). Right: number of TUNEL-positive cardiomyocytes 4 weeks after doxorubicin treatment. *P<0.05 vs saline-treated wild type mice; #P<0.05 vs doxorubicin-treated wild type mice.

phospho-ATM levels, p53 accumulation (Fig. 2(C)), and apoptotic cell death of myocytes as assessed by Bax/Bcl2 ratio and the number of TUNEL-positive cells (Figs. 2(C) and (D)). These data collectively suggest that doxorubicin treatment induces p53 accumulation via oxidative DNA damage-ATM pathway in cardiac myocytes.
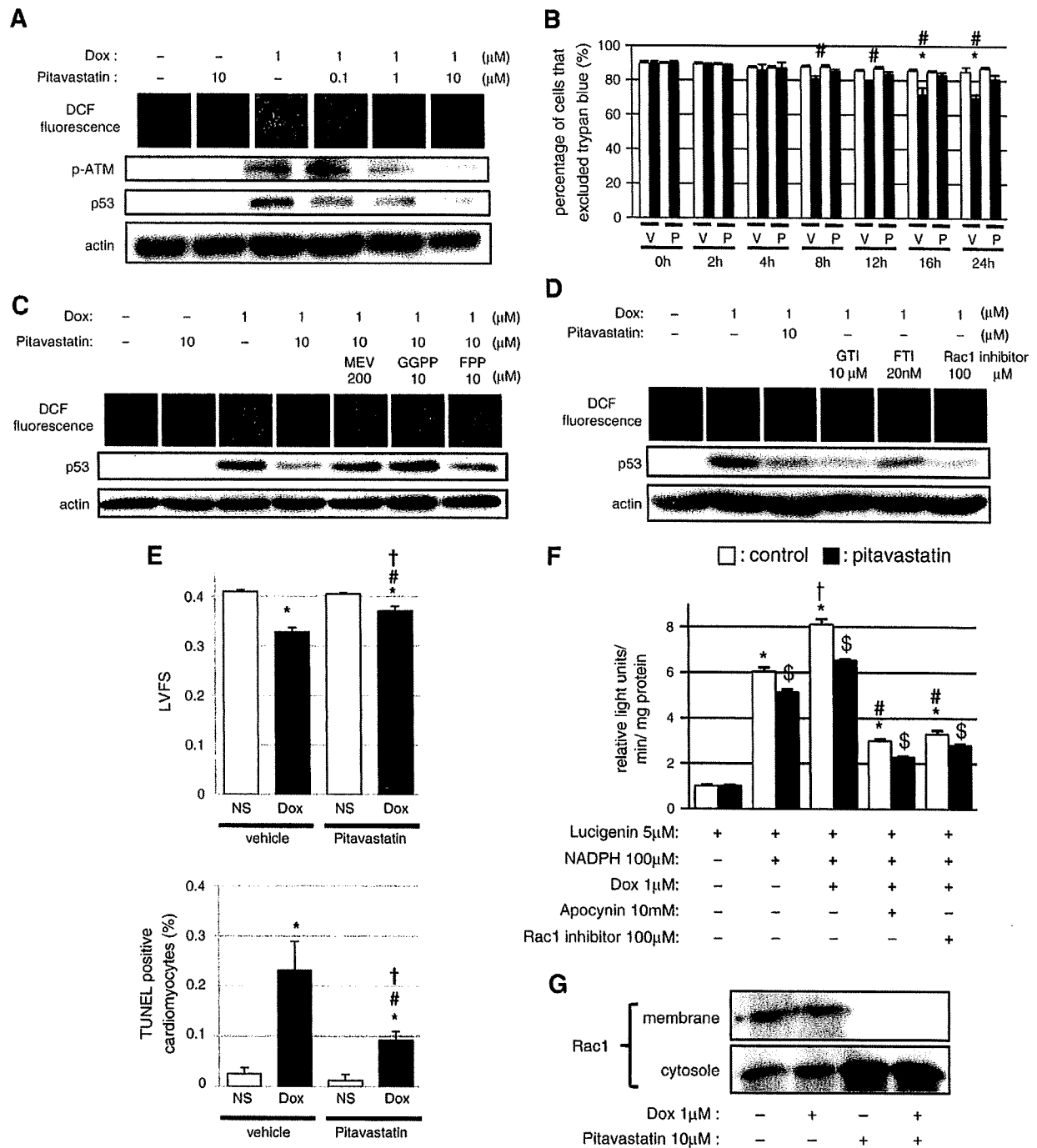

Fig. 4. Pitavastatin attenuates doxorubicin cardiotoxicity through its antioxidant effect involving Rac1 inhibition. (A) Pitavastatin attenuates doxorubicin-induced oxidative stress, ATM activation, and p53 accumulation in vitro. Oxidative stress was assessed by DCF fluorescence, and ATM activation and p53 accumulation were assessed by Western blot analysis. (B) Pitavastatin attenuates doxorubicin-induced myocyte death as assessed by trypan blue exclusion assay. White columns and black columns represent control (saline-treated) group and doxorubicin-treated group, and V and P represent vehicle and pitavastatin treatment, respectively. #$P<0.05$ vs vehicle-treated control group at the same time points; *$P<0.05$ vs pitavastatin-treated doxorubicin group at the same time points. (C) Intermediate products of the mevalonate pathway reverse the beneficial effects of pitavastatin on doxorubicin cardiotoxicity. MEV, mevalonate. (D) GTI and Rac1 inhibitor but not FTI exhibit protective effects on doxorubicin cardiotoxicity. (E) Pitavastatin attenuates doxorubicin-induced cardiomyopathy. Top: left ventricular fractional shortening of mice treated with normal saline (NS) or doxorubicin (Dox). Mice were further divided into vehicle-treated group or pitavastatin-treated group. Bottom: number of TUNEL-positive cardiomyocytes 4 weeks after doxorubicin treatment. *$P<0.05$ vs saline/vehicle-treated group; #$P<0.05$ vs saline/pitavastatin-treated group; †$P<0.05$ vs doxorubicin/vehicle-treated group. (F) Pitavastatin attenuates NADPH oxidase activity. White columns and black columns represent control (saline-treated) group and pitavastatin-treated group, respectively. *$P<0.05$ vs lucigenin-treated control group; †$P<0.05$ vs lucigenin/NADPH-treated control group; #$P<0.05$ vs lucigenin/NADPH/doxorubicin-treated control group; $P<0.05$ vs control group with the same treatment. (G) Pitavastatin inhibits translocation of Rac1 to plasma membrane. Molecular weight of Rac1 is 22 kDa.

52

3.2. Doxorubicin cardiotoxicity is mediated by p53-dependent cardiomyocyte apoptosis

We next examined the role of p53-dependent cardiomyocyte apoptosis in doxorubicin-induced cardiotoxicity in vivo. After chronic doxorubicin treatment, contractile function was impaired and apoptotic cardiomyocyte death was increased compared with vehicle treatment group in wild type mice (Fig. 3(A)). The deleterious effects of doxorubicin were attenuated in p53 heterozygous knockout mice, suggesting that p53 accumulation plays a causal role in doxorubicin cardiotoxicity (Fig. 3(B)). p53-induced cardiomyocyte apoptosis, myocardial ischemia, and mTOR inhibition have been implicated in the pathogenesis of various forms of heart failure [1,2,7,8]. However, doxorubicin cardiotoxicity was attenuated by cardiac-specific over-expression of anti-apoptotic protein Bcl-2 (Fig. 3(C)), whereas myocardial vessel density or myocyte size was not altered by chronic doxorubicin treatment (data not shown). Thus, doxorubicin cardiotoxicity is mediated by p53-dependent cardiomyocyte apoptosis.

3.3. Pitavastatin attenuates doxorubicin cardiotoxicity through its antioxidant effect involving Rac1 inhibition

Because oxidative stress is a critical inducer of p53 accumulation in the heart by doxorubicin and statins have been shown to have antioxidant effects, we examined whether pitavastatin exerts protective effects on doxorubicin cardiotoxicity. Pretreatment with pitavastatin attenuated doxorubicin-induced oxidative stress, ATM phosphorylation, p53 accumulation, and cardiomyocyte death (Figs. 4(A) and (B)). Statins are known to exert their lipid lowering-independent effects by inhibiting the synthesis of isoprenoids that are critical for posttranslational modification of a variety of proteins [9]. We therefore tested whether pitavastatin attenuates doxorubicin cardiotoxicity through the inhibition of mevalonate-dependent posttranslational protein modifications. Pretreatment with mevalonate, FPP, or GGPP reversed the beneficial effects of pitavastatin on doxorubicin-induced oxidative stress and p53 accumulation (Fig. 4(C)). Likewise, GTI but not FTI reduced doxorubicin-induced oxidative stress and p53 accumulation (Fig. 4(D)), suggesting that the inhibition of protein geranylgeranylation mediates the cardioprotective effects of pitavastatin. Because Rac1 is a major regulator of NADPH oxidase activity and activated by geranylgeranylation but not by farnesylation [14], we next examined the possible involvement of Rac1 in pitavastatin-mediated protective effects against doxorubicin. Indeed, treatment with a Rac1 inhibitor also attenuated doxorubicin-induced oxidative stress and p53 accumulation to the extent comparable with those of pitavastatin and GTI (Fig. 4(D)). Finally, treatment with pitavastatin significantly attenuated chronic doxorubicin treatment-induced cardiomyocyte apoptosis and contractile dysfunction in vivo (Fig. 4(E)), which is consistent with a recent report by others [23]. In cultured myocytes, doxorunbicin augmented NADPH oxidase activity, which was attenuated both by a NADPH oxidase assembly inhibitor (apocynin) and a Rac1 inhibitor (Fig. 4(F)). Furthermore, pitavastatin attenuated Rac1 activity as assessed by subcellular localization (Fig. 4(G)). These results collectively suggest that pitavastatin attenuates doxorubicin cardiotoxicity through its antioxidant effect involving Rac1 inhibition.

4. Discussion

4.1. Doxorubicin induces p53 accumulation in cardiac myocytes through oxidative DNA damage-ATM pathway

Several lines of evidence suggest that oxidative stress and p53 accumulation are involved in doxorubicin-induced cardiotoxicity [1,2]. Consistent with this notion, doxorubicin treatment induced oxidative stress and p53 accumulation both in vitro and in vivo, and reduction of oxidative stress by NAC treatment reduced doxorubicin-

induced p53 accumulation in vitro. Because DNA damage is induced by doxorubicin and is a potent inducer of p53 in other cell types [21], we examined whether DNA damage mediates doxorubicin-induced p53 accumulation in cardiac myocytes. Indeed, doxorubicin treatment induced DNA damage and ATM activation, and an ATM kinase inhibitor wortmannin reduced p53 accumulation induced by doxorubicin. These findings are consistent with the notion that ATM activated by DNA damage phosphorylates and stabilizes p53 protein, and suggest that doxorubicin induces p53 accumulation via oxidative DNA damage-ATM pathway. However, it should be noted that p53 accumulation is not completely inhibited by treatment with NAC or wortmannin. It was also reported that the cardioprotective effects of antioxidants are not very remarkable in human clinical trials [24]. Thus, oxidative stress-independent mechanisms may also play a role in doxorubicin-induced p53 accumulation.

4.2. Chronic doxorubicin cardiotoxicity is mediated by p53-dependent cardiomyocyte apoptosis

Previous studies have shown that doxorubicin treatment induces p53 accumulation in the heart, and reduction of p53 activity attenuates deleterious effects of doxorubicin [5,6], suggesting that p53 plays a causal role in doxorubicin cardiotoxicity. Because doxorubicin-induced myocyte apoptosis was reduced by the inhibition of p53 activity, p53-dependent cardiomyocyte apoptosis has been thought to play a crucial role in doxorubicin cardiotoxicity. However, we have recently shown that p53 inhibits the action of hypoxia-inducible factor-1 (Hif-1) and Hif-1-dependent coronary angiogenesis in the heart under chronic pressure overload, leading to contractile dysfunction [7]. More recently, it was shown that p53-induced inhibition of mTOR activity mediates acute doxorubicin cardiotoxicity independently of cardiomyocyte apoptosis [8]. These results suggest that p53-dependent but apoptosis-independent mechanisms may be involved in the pathogenesis of doxorubicin cardiotoxicity. We therefore re-evaluated the role of cardiomyocyte apoptosis in doxorubicin cardiotoxicity using transgenic mice in which cardiomyocyte apoptosis is inhibited by the over-expression of Bcl-2 in the heart, and found that inhibition of myocardial apoptosis significantly improved contractile dysfunction induced by chronic doxorubicin treatment. We also found that doxorubicin treatment did not result in myocardial hypoxia or reduction in myocyte size. Thus, we conclude that chronic doxorubicin cardiotoxicity is mediated by p53-dependent cardiomyocyte apoptosis. These data collectively suggest that, although both acute and chronic doxorubicin cardiotoxicity are mediated by p53, the downstream effectors of p53 in these two situations may be partly distinct. This notion is supported by a transcriptome analysis of acute and chronic doxorubicin cardiotoxicity, in which a different set of genes were up- or down-regulated in the heart after acute and chronic doxorubicin treatment, respectively [25]. It should also be noted that in tumor cell lines, DNA damage induces both p53-dependent and p53-independent apoptosis [26]. Whether DNA damage-dependent p53-independent apoptosis plays a role in doxorubicin cardiotoxicity remains to be elucidated.

4.3. Pitavastatin attenuates doxorubicin cardiotoxicity by inhibiting Rac1 activity

HMG-CoA reductase inhibitors or statins are widely prescribed drugs that inhibit the rate-limiting enzyme for cholesterol synthesis in the liver and lower serum cholesterol levels. However, these drugs also exert cholesterol lowering-independent or pleiotropic effects, many of which are thought to be mediated by their ability to inhibit the synthesis of isoprenoid intermediates required for posttranslational protein modifications. Specifically, isoprenylation of small G proteins such as Ras, Rho or Rac are critical for their proper membrane localization and function, and statin-mediated inhibition of these small G proteins may play a role in the pleiotropic effects of statins. Indeed, our in vitro studies

using isoprenoid intermediates and pharmacological inhibitors strongly suggest that inhibition of Rac1 activation by pitavastatin plays a crucial role in the protective effects of pitavastatin on doxorubicin cardiotoxicity. Because Rac1 is a requisite component of NADPH oxidase, our findings collectively suggest that pitavastatin attenuates doxorubicin cardiotoxicity through its antioxidant effect involving Rac1 inhibition. It was previously shown that oxidative stress is implicated in cardiac hypertrophy and that statins attenuate myocardial hypertrophy through Rac1 inhibition [12], suggesting that similar mechanisms may be involved in the pathogenesis of cardiac hypertrophy and doxorubicin cardiotoxicity.

In summary, we have shown that doxorubicin cardiotoxicity is mediated by oxidative DNA damage-ATM-p53-apoptosis pathway in vitro and in vivo, and attenuated by pitavastatin through its anti-oxidant effect involving Rac1 inhibition. Further clinical studies are mandatory to determine whether statins are really cardioprotective in the setting of anticancer therapy using doxorubicin or related chemo-therapeutic agents.

Acknowledgments

References

[1] Minotti G, Menna P, Salvatorelli E, Cairo G, Gianni L. Anthracyclines: molecular advances and pharmacologic developments in antitumor activity and cardiotoxicity. Pharmacol Rev 2004 Jun;56(2):185–229.

[2] Takemura G, Fujiwara H. Doxorubicin-induced cardiomyopathy from the cardiotoxic mechanisms to management. Prog Cardiovasc Dis 2007 Mar–Apr;49(5):330–52.

[3] Yen HC, Oberley TD, Vichitbandha S, Ho YS, St Clair DK. The protective role of manganese superoxide dismutase against adriamycin-induced acute cardiac toxicity in transgenic mice. J Clin Invest 1996 Sep 1;98(5):1253–60.

[4] Sun X, Zhou Z, Kang YJ. Attenuation of doxorubicin chronic toxicity in metallo-thionein-overexpressing transgenic mouse heart. Cancer Res 2001 Apr 15;61(8):3382–7.

[5] Liu X, Chua CC, Gao J, Chen Z, Landy CL, Hamdy R, et al. Pifithrin-alpha protects against doxorubicin-induced apoptosis and acute cardiotoxicity in mice. Am J Physiol Heart Circ Physiol 2004 Mar;286(3):H933–9.

[6] Shizukuda Y, Matoba S, Mian OY, Nguyen T, Hwang PM. Targeted disruption of p53 attenuates doxorubicin-induced cardiac toxicity in mice. Mol Cell Biochem 2005 May;273(1–2):25–32.

[7] Sano M, Minamino T, Toko H, Miyauchi H, Orimo M, Qin Y, et al. p53-induced inhibition of Hif-1 causes cardiac dysfunction during pressure overload. Nature 2007 Mar 22;446(7134):444–8.

[8] Zhu W, Soonpaa MH, Chen H, Shen W, Payne RM, Liechty EA, et al. Acute doxorubicin cardiotoxicity is associated with p53-induced inhibition of the mammalian target of rapamycin pathway. Circulation 2009 Jan 6;119(1):99–106.

[9] Mital S, Liao JK. Statins and the myocardium. Semin Vasc Med 2004 Nov;4(4):377–84.

[10] Endres M, Laufs U, Huang Z, Nakamura T, Huang P, Moskowitz MA, et al. Stroke protection by 3-hydroxy-3-methylglutaryl (HMG)-CoA reductase inhibitors mediated by endothelial nitric oxide synthase. Proc Natl Acad Sci U S A 1998 Jul 21;95(15):8880–5.

[11] Lefer AM, Campbell B, Shin YK, Scalia R, Hayward R, Lefer DJ. Simvastatin pre-serves the ischemic-reperfused myocardium in normocholesterolemic rat hearts. Circulation 1999 Jul 13;100(2):178–84.

[12] Takemoto M, Node K, Nakagami H, Liao Y, Grimm M, Takemoto Y, et al. Statins as antioxidant therapy for preventing cardiac myocyte hypertrophy. J Clin Invest 2001 Nov;108(10):1429–37.

[13] Hasegawa H, Yamamoto R, Takano H, Mizukami M, Asakawa M, Nagai T, et al. 3-Hydroxy-3-methylglutaryl coenzyme A reductase inhibitors prevent the development of cardiac hypertrophy and heart failure in rats. J Mol Cell Cardiol 2003 Aug;35(8):953–60.

[14] Groemping Y, Rittinger K. Activation and assembly of the NADPH oxidase: a structural perspective. Biochem J 2005 Mar 15;386(Pt 3):401–16.

[15] Zou Y, Komuro I, Yamazaki T, Kudoh S, Uozumi H, Kadowaki T, et al. Both Gs and Gi proteins are critically involved in isoproterenol-induced cardiomyocyte hypertrophy. J Biol Chem 1999 Apr 2;274(14):9760–70.

[16] Tanaka M, Nakae S, Terry RD, Mokhtari GK, Gunawan F, Balsam LB, et al. Cardiomyocyte-specific Bcl-2 overexpression attenuates ischemia-reperfusion injury, immune response during acute rejection, and graft coronary artery disease. Blood 2004 Dec 1;104(12):3789–96.

[17] Li SY, Gomelsky M, Duan J, Zhang Z, Gomelsky L, Zhang X, et al. Overexpression of aldehyde dehydrogenase-2 (ALDH2) transgene prevents acetaldehyde-induced cell injury in human umbilical vein endothelial cells: role of ERK and p38 mitogen-activated protein kinase. J Biol Chem 2004 Mar 19;279(12):11244–52.

[18] Szocs K, Lassegue B, Sorescu D, Hilenski LL, Valppu L, Couse TL, et al. Upregulation of Nox-based NAD(P)H oxidases in restenosis after carotid injury. Arterioscler Thromb Vasc Biol 2002 Jan;22(1):21–7.

[19] Deng S, Kruger A, Kleschyov AL, Kalinowski L, Daiber A, Wojnowski L. Gp91phox-containing NAD(P)H oxidase increases superoxide formation by doxorubicin and NADPH. Free Radic Biol Med 2007 Feb 15;42(4):466–73.

[20] Spallarossa P, Garibaldi S, Altieri P, Fabbi P, Manca V, Nasti S, et al. Carvedilol prevents doxorubicin-induced free radical release and apoptosis in cardiomyo-cytes in vitro. J Mol Cell Cardiol 2004 Oct;37(4):837–46.

[21] L'Ecuyer T, Sanjeev S, Thomas R, Novak R, Das L, Campbell W, et al. DNA damage is an early event in doxorubicin-induced cardiac myocyte death. Am J Physiol Heart Circ Physiol 2006 Sep;291(3):H1273–80.

[22] Kurz EU, Douglas P, Lees-Miller SP. Doxorubicin activates ATM-dependent phosphorylation of multiple downstream targets in part through the generation of reactive oxygen species. J Biol Chem 2004 Dec 17;279(51):53272–81.

[23] Riad A, Bien S, Westermann D, Becher PM, Loya K, Landmesser U, et al. Pretreat-ment with statin attenuates the cardiotoxicity of Doxorubicin in mice. Cancer Res 2009 Jan 15;69(2):695–9.

[24] Ladas EJ, Jacobson JS, Kennedy DD, Teel K, Fleischauer A, Kelly KM. Antioxidants and cancer therapy: a systematic review. J Clin Oncol 2004 Feb 1;22(3):517–28.

[25] Yi X, Bekeredjian R, DeFilippis NJ, Siddiquee Z, Fernandez E, Shohet RV. Transcriptional analysis of doxorubicin-induced cardiotoxicity. Am J Physiol Heart Circ Physiol 2006 Mar;290(3):H1098–102.

[26] Roos WP, Kaina B. DNA damage-induced cell death by apoptosis. Trends Mol Med 2006 Sep;12(9):440–50.

Transplantation of cardiac progenitor cells ameliorates cardiac dysfunction after myocardial infarction in mice

Katsuhisa Matsuura,[1,2] Atsushi Honda,[1] Toshio Nagai,[3] Noritoshi Fukushima,[1] Koji Iwanaga,[3] Masakuni Tokunaga,[3] Tatsuya Shimizu,[2] Teruo Okano,[2] Hiroshi Kasanuki,[1] Nobuhisa Hagiwara,[1] and Issei Komuro[3]

[1]Department of Cardiology and [2]Institute of Advanced Biomedical Engineering and Science, Tokyo Women's Medical University, Tokyo, Japan. [3]Department of Cardiovascular Science and Medicine, Chiba University Graduate School of Medicine, Chiba, Japan.

Cardiac progenitor cells are a potential source of cell therapy for heart failure. Although recent studies have shown that transplantation of cardiac stem/progenitor cells improves function of infarcted hearts, the precise mechanisms of the improvement in function remain poorly understood. The present study demonstrates that transplantation of sheets of clonally expanded stem cell antigen 1–positive (Sca-1–positive) cells (CPCs) ameliorates cardiac dysfunction after myocardial infarction in mice. CPC efficiently differentiated into cardiomyocytes and secreted various cytokines, including soluble VCAM-1 (sVCAM-1). Secreted sVCAM-1 induced migration of endothelial cells and CPCs and prevented cardiomyocyte death from oxidative stress through activation of Akt, ERK, and p38 MAPK. Treatment with antibodies specific for very late antigen-4 (VLA-4), a receptor of sVCAM-1, abolished the effects of CPC-derived conditioned medium on cardiomyocytes and CPCs in vitro and inhibited angiogenesis, CPC migration, and survival in vivo, which led to attenuation of improved cardiac function following transplantation of CPC sheets. These results suggest that CPC transplantation improves cardiac function after myocardial infarction through cardiomyocyte differentiation and paracrine mechanisms mediated via the sVCAM-1/VLA-4 signaling pathway.

Introduction

Accumulating evidence has suggested that myocardial regeneration is a promising therapy for various heart diseases (1). Recently, several groups, including our own, have reported that adult hearts contain cardiac stem/progenitor cells that can differentiate into functional cardiomyocytes in vitro and in vivo (2–6). Transplantation of cardiac stem/progenitor cells has been shown to improve cardiac function via newly formed cardiomyocytes and blood vessels (2, 7). On the other hand, it has been reported that when noncardiac stem cells are transplanted, paracrine factors play a major role in the improvement of cardiac function (8, 9). Several preclinical reports and clinical trials have demonstrated that intracoronary or intramyocardial injection of bone marrow–derived cells attenuates cardiac dysfunction following acute and chronic myocardial infarction (MI) (10–12). However, it is not known whether cardiac stem/progenitor cells are superior to other noncardiac stem/progenitor cells. Furthermore, it remains unclear to what extent paracrine effects or transdifferentiation of cardiac stem/progenitor cells contributes to beneficial effects on cardiac function.

Transplanted cells are the source of paracrine factors or newly formed cardiomyocytes, and the survival of grafted cells is a critical issue. The majority of the grafted cells have been reported to disappear within 1 week after transplantation when directly injected into ischemic hearts (9, 13), suggesting that alternative strategies to facilitate survival of grafted cells are required. We developed temperature-responsive culture dishes that were covalently grafted with the temperature-responsive polymer poly(N-isopropylacrylamide) (PIPAAm) (14). Lowering the temperature induces a rapid surface transition from hydrophobic (cell adhesive) to hydrophilic (non–cell adhesive), which results in the release of contiguous viable cell sheets with full preservation of cell-to-cell connections and adhesion proteins without using any enzymatic digestion (15). To date, cell sheet transplantations of skeletal myoblasts (16), mesenchymal stem cells derived from adipose tissue (17), and menstrual blood (18) have been reported to improve cardiac function in animal MI models. However, the precise mechanisms of the improvement, which include mutual interactions between host tissue and transplanted cells, remain poorly understood.

The present study demonstrates that transplanted cell sheets of clonally expanded stem cell antigen 1–positive (Sca-1–positive) cells (CPCs) differentiated into cardiomyocytes and vascular cells and prevented cardiac remodeling after MI. CPCs secreted soluble VCAM-1 (sVCAM-1), which facilitated engraftment and migration of CPCs from cell sheets into host myocardium and improved cardiac function after MI via angiogenic and cardioprotective effects mediated by paracrine mechanisms.

Results

Establishment and character of CPCs. Since primary isolated Sca-1–positive cells, which were derived from adult murine hearts, con-

55

sisted of several cell populations, including cardiac stem/progenitor cells, hematopoietic cells, and endothelial cells (ref. 4 and our unpublished observations), clonal cells were initially established from cardiac Sca-1-positive cells. A total of 10^4 primary isolated Sca-1-positive cells derived from adult murine hearts were plated onto 10-cm culture dishes. After repeated limited dilutions, clonal cell lines were established. The efficiency of cloning was approximately 0.1%. The clonal cells were expanded for more than 500 population doublings (Figure 1A). Flow cytometric analysis revealed that almost 100% of cells expressed Sca-1, CD29, and CD44, approximately 20% of cells expressed CD34, and no cells expressed CD31, CD45, and c-kit throughout the culture passages (Table 1 and Supplemental Figure 1; supplemental material available online with this article; doi:10.1172/JCI37456DS1), suggesting that the clonal cells were not homogenous. Under culture conditions of 80% confluency, the clonal cells expressed cardiac transcription factors, such as Nkx2.5 and GATA4 (Figure 1B), but not cardiac contractile proteins. These cell phenotypes remained unchanged throughout the culture passages. Gene profiles and cell-surface marker analyses revealed that CPCs were similar to primary isolated Sca-1-positive cells in analyses previously reported (4). Therefore, CPCs possessed features almost identical to those of intrinsic cardiac stem/progenitor cells. When CPCs were cultured under confluent conditions for 4 weeks, expression levels of Nkx2.5 and GATA4 were upregulated and expressions of myocyte enhancer factor 2C (MEF2C), atrial natriuretic peptide (ANP), β-myosin heavy chain (β-MHC), and sarcomeric α-actinin were detected at mRNA and protein levels (Figure 1, B and C). These results suggested that CPCs differentiated into immature cardiomyocytes in vitro. However, the cells did not exhibit spontaneous beating. To examine the cardiac differentiation potency of CPCs in vivo, 2.0×10^6 CPCs labeled with red fluorescent protein (RFP) were injected directly into the infarcted myocardium within 5 minutes after left coronary artery ligation. At 4 weeks after transplantation, several GATA4-expressing RFP+ cells were recognized in the border areas and some RFP+ cells expressed sarcomeric α-actinin in a fine striated pattern, which suggested that CPCs differentiated into mature cardiomyocytes in vivo (Figure 1, D and E). However, transplanted CPC-derived RFP expression in the infarcted heart was very weak 1 week after transplantation compared with immediately after transplantation (Supplemental Figure 2). These results suggest that direct intramyocardial injection is not an ideal method for efficient engraftment.

Cell sheet transplantation. To elucidate the functional benefits of CPC transplantation in the infarcted heart compared with effects of noncardiac stem/progenitor cells, cell sheet transplantation methods were utilized. RFP+ CPCs or adipose tissue-derived mesenchymal cells (ATMCs) isolated from GFP mice were cultured on temperature-responsive culture dishes at 37°C. The monolayered cell sheet was collected by decreasing the temperature at which it was cultured to 20°C. Final cell counts and areas of monolayered cell sheets prior to transplantation were $2.0 \pm 0.2 \times 10^6$ cells and 80.1 ± 3.3 mm^2 in CPCs and $1.9 \pm 0.1 \times 10^6$ cells and 79.3 ± 2.0 mm^2 in ATMCs, respectively ($n = 5$). The mice were randomly assigned into 3 groups: mice transplanted with monolayered CPCs (CPC group), mice transplanted with monolayered ATMCs (ATMC group), and mice that were not transplanted (MI group). Within 5 minutes after left coronary artery ligation, monolayered CPC or ATMC sheets were transplanted over the infarcted area and cardiac function was examined by echocardiography every week. Echocar-

diographic analysis revealed that LV diastolic dimension (LVDd) and LV systolic dimension (LVDs) were significantly decreased at 4 weeks and fractional shortening (FS) was markedly improved 3 weeks after transplantation in the CPC group compared with the MI and ATMC groups. These results suggested that transplantation of CPC sheets inhibited cardiac remodeling and improved cardiac function following MI (Figure 2A). Furthermore, LV end-diastolic pressure (LVEDP) and +dp/dt, as determined by catheter, were markedly improved in the CPC group compared with the remaining 2 groups at 4 weeks (Figure 2B). In contrast, in the ATMC group, LVDs was significantly smaller and FS was better 1 week after transplantation compared with the MI and CPC groups. However, these favorable effects were not observed 2 weeks after transplantation, and cardiac remodeling and dysfunction progressed in a manner similar to that in the MI group (Figure 2A). The fibrotic area, which was evaluated by Masson trichrome staining 4 weeks after transplantation, was significantly smaller in the CPC group compared with the other 2 groups (Figure 3A). At 1 week after transplantation, more vWF-positive blood vessels were observed in the border area of the ATMC group than in the MI and CPC groups (Figure 3B). At 4 weeks, a greater number of vessels were detected in the CPC group than in the MI and ATMC groups (Figure 3C). Furthermore, when lectin perfusion assay was performed at 4 weeks, more lectin-positive blood vessels were detected in the border area of the CPC group compared with the remaining 2 groups (Supplemental Figure 4). In contrast, there were few inflammatory cells in the border area of each group at 4 weeks (Supplemental Figure 5).

Cell survival and differentiation. Immunohistochemical analysis showed that many transplanted CPCs were present in the middle of the LV wall, including the normal and injured areas (normal area, 28.3 ± 9.7 cells/mm^2; injured area, 235.9 ± 75.1 cells/mm^2), after 4 weeks (Figure 4, A–C). This suggested that CPCs migrated from the epicardial cell sheet into the ventricular myocardium following transplantation. Conversely, GFP+ ATMCs were not observed in the myocardium (data not shown). Western blot analysis, using Abs against fluorescent proteins, revealed that approximately 20% of transplanted CPCs remained 4 weeks after transplantation, whereas only approximately 0.8% of transplanted ATMCs remained (Supplemental Figure 3). Furthermore, approximately 30% of RFP+ cells expressed sarcomeric α-actinin in a fine striated pattern, and some RFP+ cells also formed blood vessel structures (Figure 4, D–F). Because cardiomyocytes have the ability to fuse with surrounding noncardiomyocytes (19), the possibility that CPCs acquired cardiomyogenic features following fusion with existing cardiomyocytes was examined. When RFP+ CPC sheets were transplanted into hearts of GFP mice immediately following MI, approximately half of the α-actinin-expressing cells expressed GFP in injured areas 4 weeks after transplantation (Supplemental Figure 6, A, B, and E). In the normal areas, all of the α-actinin-expressing RFP+ cells expressed GFP (Supplemental Figure 6, C–E). To further ensure the occurrence of cell fusion, sheets of nonlabeled CPCs derived from male mice were transplanted into the infarcted hearts of female mice. At 4 weeks after transplantation, cells exhibiting a fine striated pattern possessed 3 X chromosomes and a Y chromosome in the nucleus (Supplemental Figure 7). These findings suggested that CPCs differentiated into cardiomyocytes via cell fusion–dependent and –independent mechanisms. Because approximately 20% of transplanted CPCs remained at 4 weeks (Supplemental Figure 3), approximately
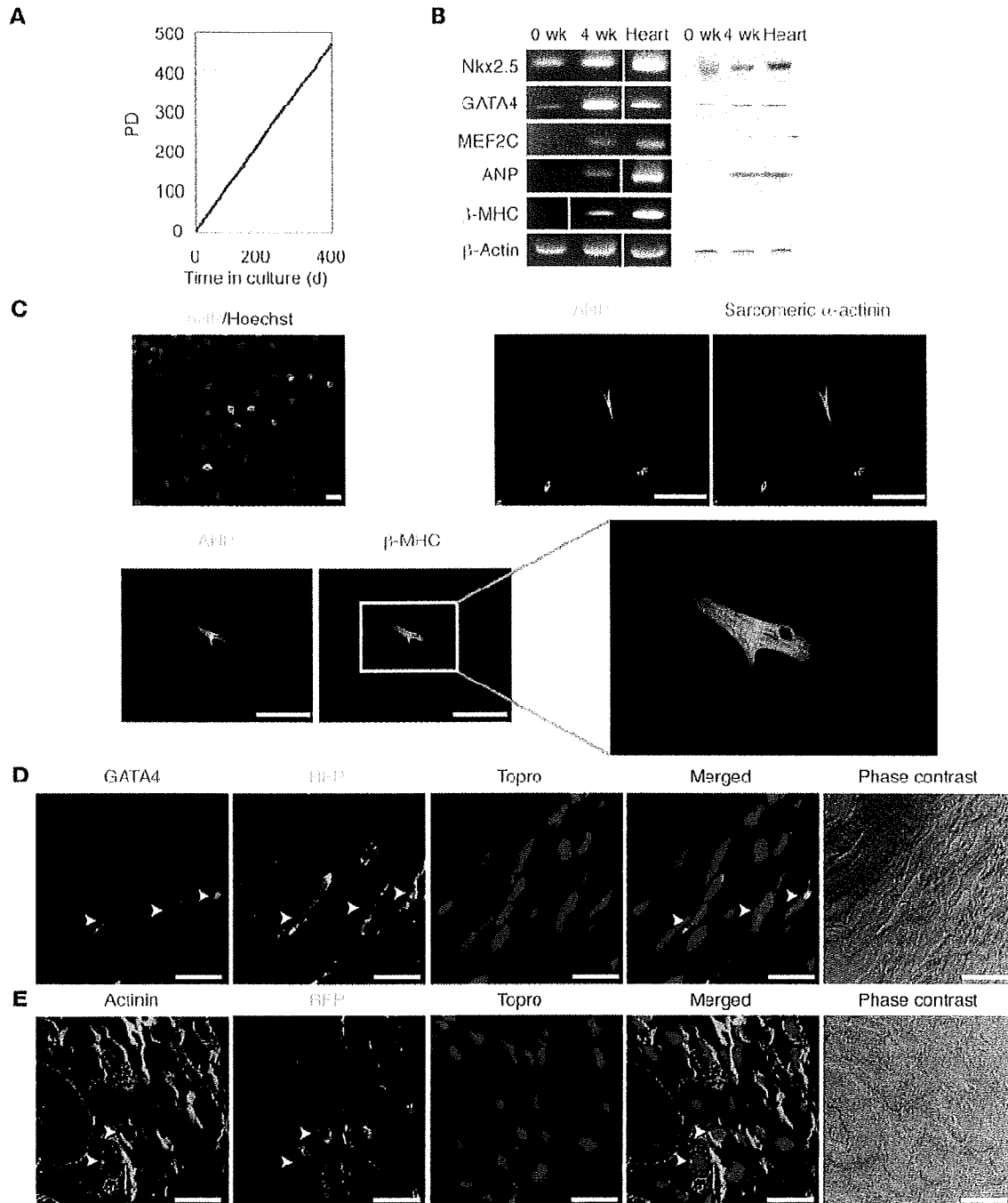
A

B

C

D

E

Figure 1

Character of CPCs. (A) CPCs were expanded more than 500 population doublings (P.D.) over a 1-year period. (B and C) Cardiac mRNA and protein expressions in CPCs. (B) Left panels show RT-PCR. Noncontiguous lanes from the same gel were spliced together into a composite band. The thin white line indicates the spliced point. Right panels show Western blot. (C) Immunofluorescent images of CPCs 4 weeks after starting culture under confluent conditions. Scale bars: 100 μm. (D and E) Confocal microscopic images of the infarcted heart 4 weeks after direct injection of RFP+ CPCs. (D) GATA4-expressing RFP+ cells (arrowheads) were recognized in the infarcted region. (E) Some RFP+ cells (arrowheads) expressed sarcomeric α-actinin in the infarcted area. Scale bars: 5 μm.

4.0 × 10⁵ out of approximately 2.0 × 10⁶ transplanted CPCs were thought to survive and undergo engraftment. As approximately 30% of survived CPCs expressed cardiac contractile proteins (Fig-

ure 4, C and E), approximately 1.2 × 10⁵ CPCs were estimated to differentiate into cardiomyocytes. Since approximately half of the cardiac protein-expressing cells resulted from cell fusion with

Table 1

The percentage of cell-surface antigens

	Sca-1	CD29	CD31	CD34	CD44	CD45	c-kit
P.D.10	99.8	99.9	0.1	15.6	100	0.5	0.4
P.D.100	95.5	99.7	0.3	42.8	100	0.2	0.3
P.D.200	99.8	100	0.1	45.5	100	0.1	0.1
P.D.300	99.8	99.9	0.2	15.5	99.9	0.4	0.2
P.D.400	100	100	0.3	27.5	100	0.3	0.4
P.D.500	99.9	99.9	0.1	15.4	100	0.5	0.5

of VCAM-1/sVCAM-1 and VEGF between CPCs and ATMCs (Figure 5A). VCAM-1 expression was almost identical among the 3 groups at 1 week. However, at 4 weeks after transplantation, expression levels remained high in the CPC group compared with the other 2 groups (Figure 5B). Time course of VCAM-1 expression was consistent with improved cardiac function (Figure 2A). Conversely, VEGF expression was significantly upregulated at 1 week in the ATMC group compared with the other groups. However, at 4 weeks, expression levels were similar among the 3 groups (Figure 5B). This was consistent with observations that transplanted ATMC sheets improved cardiac function at 1 week but not at 4 weeks (Figure 2A). The concentrations of sVCAM-1 and VEGF in peripheral blood remained unchanged in all groups 1 and 4 weeks after transplantation (Supplemental Figure 8).

existing cardiomyocytes (Supplemental Figure 6E), CPC sheet transplantation was estimated to create approximately 0.6×10^5 new cardiomyocytes in the entire heart. The number of cardiomyocytes in an adult murine heart has been estimated to be 3×10^6 (20). Therefore, approximately 5% of cardiomyocytes were regenerated and might have contributed to improved cardiac function by CPC sheet transplantation.

Secretion of growth factors. Recent reports have suggested that cell transplantation improves cardiac function after MI through the release of humoral factors (8, 9). Analyses of conditioned medium (CM) from CPCs and ATMCs using a cytokine Ab array revealed that sVCAM-1 was more abundant in CPCs, while VEGF was dominantly expressed in ATMCs (Table 2). Western blot analysis of whole-cell lysates and ELISA of CM confirmed altered expressions

CPC-derived sVCAM-1-mediated angiogenesis and cardioprotective effects. CPC-derived CM and sVCAM-1 induced greater endothelial cell migration and tube formation compared with control medium (Figure 5, C and D). sVCAM-1-depleted CM, which was obtained from CPCs transfected with VCAM-1-specific microRNA (miRNA) plasmid vector (Supplemental Figure 9, A and B), induced significantly less endothelial cell migration (Figure 5C) and tube formation (Figure 5D) compared with CPC-derived CM. This suggested that angiogenic activity of CPC-derived CM was mediated at least in part by sVCAM-1. Subsequently, the protective
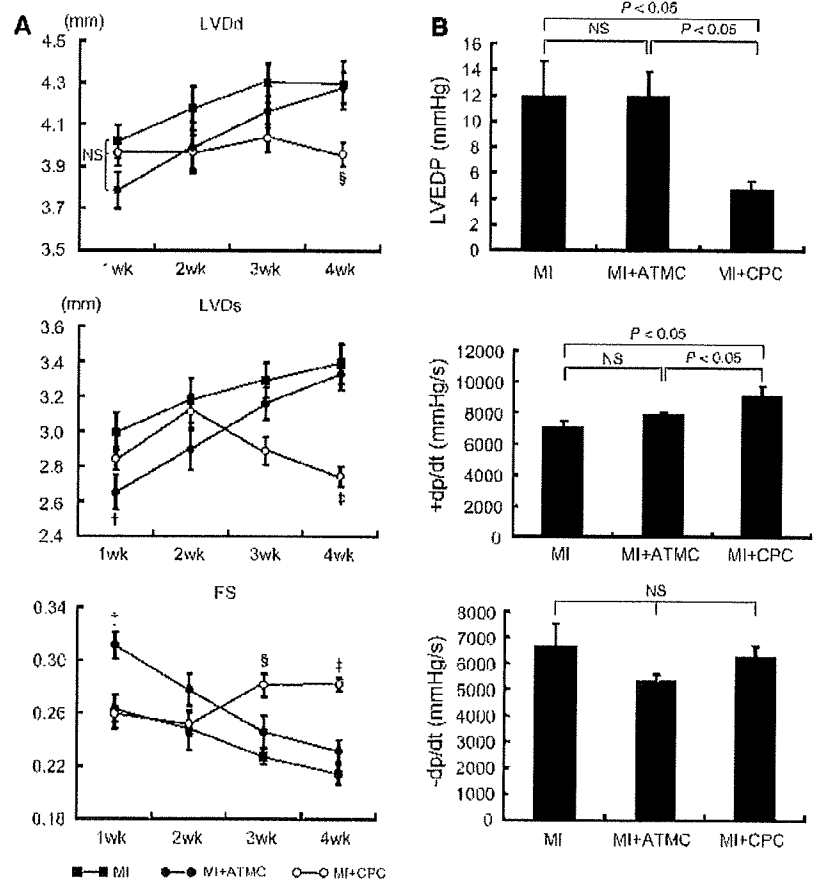

Figure 2
Effects of CPC sheet transplantation on cardiac function after MI. (A) Echocardiographic analysis. CPC sheet transplantation inhibited dilatation of LVDd and LVDs and improved FS 3 weeks later. ATMC transplantation inhibited dilatation of LVDs and FS reduction at 1 week, but not afterward. $^†P < 0.05$ versus MI or MI plus CPCs ($n = 10$ per group). $^‡P < 0.01$ versus MI or MI plus ATMCs ($n = 10$ per group). $^§P < 0.05$ versus MI or MI plus ATMCs ($n = 10$ per group). (B) Catheterization analysis at 4 weeks after transplantation. CPC sheet transplantation improved LVEDP and +dp/dt compared with that in the MI or MI plus ATMC groups ($n = 5$). Data are shown as mean ± SEM.

58